ENCLOSURE

ATTACHMENT 13.5

SIA Report No. 0801273.401

Flaw Evaluation and Vibration Assessment of the Nine Mile Point Unit 2 Steam Dryer for Extended Power Uprate Operating Conditions

Nine Mile Point Nuclear Station, LLC
May 27, 2009

Report No. 0801273.401
Revision 1
Project No. 0801273
March 2009

Flaw Evaluation and Vibration Assessment of the Nine Mile Point Unit 2 Steam Dryer for Extended Power Uprate Operating Conditions

Prepared for:

Continuum Dynamics, Inc.
Ewing, NJ
Purchase Order Number 08-509

Prepared by:

Structural Integrity Associates, Inc.
Centennial, Colorado

Prepared by: _____ Date: 3/27/09
D. V. Sommerville

Reviewed by: _____ Date: 3/27/09
S. S. Tang

Approved by: _____ Date: 3/27/09
K. K. Fujikawa, P.E.

Structural Integrity Associates, Inc.

REVISION CONTROL SHEET

Document Number: **0801273.401**

Title: Flaw Evaluation and Vibration Assessment of the Nine Mile Point Unit 2 Steam Dryer for Extended Power Uprate Operating Conditions

Client: Continuum Dynamics, Inc.

SI Project Number: **0801273** Quality Program: ☒ Nuclear ☐ Commercial

Section	Pages	Revision	Date	Comments
1	1-1	0	12/31/08	Initial Issue
2	2-1 – 2-7			
3	3-1 – 3-5			
4	4-1 – 4-11			
5	5-1 – 5-49			
6	6-1			
7	7-1			
	In computer files.			
2	2-1	1	3/27/09	Address Constellation comments
4	4-5, 4-7, 4-8, 4-11, 4-12			
5	5-1, 5-9, 5-10			

Table of Contents

Section Page

1.0 INTRODUCTION & SCOPE 1-1

2.0 OBSERVED CRACKING 2-1

3.0 INPUT DATA 3-1

3.1 Upper Support Ring Input Data 3-1

3.1.1 Upper Support Ring Geometry 3-1

3.1.2 Upper Support Ring Material 3-1

3.1.3 Upper Support Ring Boundary Conditions 3-2

3.2 Drain Channel Vertical Weld Input Data 3-2

3.2.1 Drain Channel & Skirt Geometry 3-2

3.2.2 Drain Channel & Skirt Material 3-2

3.2.3 Drain Channel & Skirt Boundary Conditions 3-3

3.3 Tie Bar Input Data 3-3

3.3.1 Tie Bar Geometry 3-3

3.3.2 Tie Bar Material 3-3

3.3.3 Tie Bar Boundary Conditions 3-3

4.0 FLAW EVALUATION 4-1

4.1 Upper Support Ring 4-1

4.1.1 Assumptions 4-1

4.1.2 Methods 4-2

4.1.3 Results 4-3

4.2 Drain Channel 4-5

4.2.1 Assumptions 4-5

4.2.2 Methods 4-6

4.2.3 Results 4-7

4.3 Tie Bars 4-9

5.0 VIBRATION ASSESSMENT 5-1
5.1 Upper Support Ring 5-1
5.1.1 Assumptions 5-1
5.1.2 Methods 5-2
5.1.3 Results 5-8
5.2 Drain Channel Vertical Weld 5-10
5.2.1 Assumptions 5-10
5.2.2 Methods 5-10
5.2.3 Results 5-11
6.0 CONCLUSIONS 6-1
7.0 REFERENCES 7-1

List of Tables

Table Page

Table 2-1. Summary of Indication Dimensions Considered in Evaluation. 2-3

Table 2-2. Apparent 1-cycle Crack Growth for Drain Channel Indications. 2-3

Table 4-1. Summary of K_I results for NMP2 Steam Dryer Indications 4-10

Table 4-2. Summary of Maximum EPU FIV Stress Intensity Along Weld DC-V3-320. 4-10

Table 5-1. Tabulation of Parametric Cracked Beam Calculations 5-13

Table 5-2. Matrix of Parametric Crack Cases Considered. 5-16

Table 5-3. Summary of Modal Frequencies < 250 Hz for Three Mesh Densities 5-16

Table 5-4. Summary of Parametric Results for Mode 1 and Ratio of Cracked / Uncracked Frequencies 5-17

Table 5-5. Summary of Parametric Results for Mode 2 and Ratio of Cracked / Uncracked Frequencies 5-18

Table 5-6. Summary of Parametric Results for Mode 3 and Ratio of Cracked / Uncracked Frequencies 5-19

Table 5-7. Summary of Parametric Results for Mode 4 and Ratio of Cracked / Uncracked Frequencies 5-20

Table 5-8. Summary of Parametric Results for Mode 5 and Ratio of Cracked / Uncracked Frequencies 5-21

Table 5-9. Summary of Parametric Results for Mode 6 and Ratio of Cracked / Uncracked Frequencies 5-22

Table 5-10. Summary of Parametric Results for Mode 7 and Ratio of Cracked / Uncracked Frequencies 5-23

Table 5-11. Summary of Parametric Results for Mode 8 and Ratio of Cracked / Uncracked Frequencies 5-24

Table 5-12. Summary of Parametric Results for Mode 9 and Ratio of Cracked / Uncracked Frequencies 5-25

Table 5-13. Summary of Parametric Results for Mode 10 and Ratio of Cracked / Uncracked Frequencies 5-26

Table 5-14. Summary of Parametric Results for Mode 11 and Ratio of Cracked / Uncracked Frequencies 5-27
Table 5-15. Summary of Parametric Results for Mode 12 and Ratio of Cracked / Uncracked Frequencies 5-28
Table 5-16. Summary of Parametric Results for Mode 13 and Ratio of Cracked / Uncracked Frequencies 5-29
Table 5-17. Summary of Parametric Results for Mode 14 and Ratio of Cracked / Uncracked Frequencies 5-30
Table 5-18. Summary of Parametric Results for Mode 15 and Ratio of Cracked / Uncracked Frequencies 5-31

List of Figures

Figure Page

Figure 2-1. Representative Photograph of Vertical Indications in Upper Support Ring. 2-4
Figure 2-2. Representative Photograph of Horizontal Indications in Upper Support Ring. 2-4
Figure 2-3. INF-08-21 Photograph of DC-V3-320 Indication E [1]. 2-5
Figure 2-4. INF-08-21 Photograph of DC-V3-320 Indication H [1]. 2-5
Figure 2-5. INF-08-22 Photograph of DC-V7-140 Indication G [1]. 2-6
Figure 2-6. Representative Photograph of Tie Bar Cracking. 2-6
Figure 2-7. Representative Photograph of Tie Bar Cracking. 2-7
Figure 3-1. NMP2 Steam Dryer Model Showing Upper Support Ring, Drain Channel, and Skirt. 3-4
Figure 3-2. Orientation of Tie Bars on Steam Dryer Assembly [4]. 3-5
Figure 4-1. Reference Fatigue Crack Growth Curves for Austenitic Stainless Steels in Air Environments [Fig. C-8410-1, 7]. 4-11
Figure 4-2. NMP2 EPU FIV Stress Intensity Along Weld DC-V3-320. 4-12
Figure 4-3. NMP2 EPU FIV Stress Intensity Along and Adjacent to Weld DC-V3-320. 4-12
Figure 5-1. Composite Beam Composed of 1 Cracked and 1 Uncracked Section. 5-14
Figure 5-2. Ratio of Effective Elastic Modulus to Uncracked Elastic Modulus for a Cracked Beam for Various a/W and δ/L. 5-15
Figure 5-3. Ratio of Effective Elastic Modulus to Uncracked Elastic Modulus for a Cracked Beam for Various a/W and δ/L, Zoomed to NMP2 Effective δ/L. 5-15
Figure 5-4. Ratio of Cracked / Uncracked Frequency, Mode 1. 5-17
Figure 5-5. Ratio of Cracked / Uncracked Frequency, Mode 2. 5-18
Figure 5-6. Ratio of Cracked / Uncracked Frequency, Mode 3. 5-19
Figure 5-7. Ratio of Cracked / Uncracked Frequency, Mode 4. 5-20
Figure 5-8. Ratio of Cracked / Uncracked Frequency, Mode 5. 5-21
Figure 5-9. Ratio of Cracked / Uncracked Frequency, Mode 6. 5-22
Figure 5-10. Ratio of Cracked / Uncracked Frequency, Mode 7. 5-23
Figure 5-11. Ratio of Cracked / Uncracked Frequency, Mode 8. 5-24
Figure 5-12. Ratio of Cracked / Uncracked Frequency, Mode 9. 5-25

Figure 5-13. Ratio of Cracked / Uncracked Frequency, Mode 10 5-26
Figure 5-14. Ratio of Cracked / Uncracked Frequency, Mode 11 5-27
Figure 5-15. Ratio of Cracked / Uncracked Frequency, Mode 12 5-28
Figure 5-16. Ratio of Cracked / Uncracked Frequency, Mode 13 5-29
Figure 5-17. Ratio of Cracked / Uncracked Frequency, Mode 14 5-30
Figure 5-18. Ratio of Cracked / Uncracked Frequency, Mode 15 5-31
Figure 5-19. Crack Configuration Evaluated for NMP2 Drain Channel Cracking.. 5-32
Figure 5-20. Mesh Density and Boundary Conditions Selected for Modal Analysis of Cracked Panel 5-32
Figure 5-21. Sample Panel Area Showing Location of Crack in Panel. 5-33
Figure 5-22. Modal Comparison Between Uncracked (Top) and Cracked (Bottom) Panels, Mode 1, x/H=0.4, a/W=0.1. 5-34
Figure 5-23. Modal Comparison Between Uncracked (Top) and Cracked (Bottom) Panels, Mode 2, x/H=0.4, a/W=0.1. 5-35
Figure 5-24. Modal Comparison Between Uncracked (Top) and Cracked (Bottom) Panels, Mode 3, x/H=0.4, a/W=0.1. 5-36
Figure 5-25. Modal Comparison Between Uncracked (Top) and Cracked (Bottom) Panels, Mode 4, x/H=0.4, a/W=0.1. 5-37
Figure 5-26. Modal Comparison Between Uncracked (Top) and Cracked (Bottom) Panels, Mode 5, x/H=0.4, a/W=0.1. 5-38
Figure 5-27. Modal Comparison Between Uncracked (Top) and Cracked (Bottom) Panels, Mode 6, x/H=0.4, a/W=0.1. 5-39
Figure 5-28. Modal Comparison Between Uncracked (Top) and Cracked (Bottom) Panels, Mode 7, x/H=0.4, a/W=0.1. 5-40
Figure 5-29. Modal Comparison Between Uncracked (Top) and Cracked (Bottom) Panels, Mode 8, x/H=0.4, a/W=0.1. 5-41
Figure 5-30. Modal Comparison Between Uncracked (Top) and Cracked (Bottom) Panels, Mode 9, x/H=0.4, a/W=0.1. 5-42
Figure 5-31. Modal Comparison Between Uncracked (Top) and Cracked (Bottom) Panels, Mode 10, x/H=0.4, a/W=0.1. 5-43

Figure 5-32. Modal Comparison Between Uncracked (Top) and Cracked (Bottom) Panels, Mode 11, x/H=0.4, a/W=0.1. 5-44
Figure 5-33. Modal Comparison Between Uncracked (Top) and Cracked (Bottom) Panels, Mode 12, x/H=0.4, a/W=0.1. 5-45
Figure 5-34. Modal Comparison Between Uncracked (Top) and Cracked (Bottom) Panels, Mode 13, x/H=0.4, a/W=0.1. 5-46
Figure 5-35. Modal Comparison Between Uncracked (Top) and Cracked (Bottom) Panels, Mode 14, x/H=0.4, a/W=0.1. 5-47
Figure 5-36. Modal Comparison Between Uncracked (Top) and Cracked (Bottom) Panels, Mode 15, x/H=0.4, a/W=0.1. 5-48
Figure 5-37. Modal Comparison Between Uncracked (Top) and Cracked (Bottom) Panels, Mode 15, x/H=0.4, a/W=0.3. 5-49

1.0 INTRODUCTION & SCOPE

Constellation Energy Group has contracted with Continuum Dynamics, Incorporated (CDI) to perform a stress analysis of the Nine Mile Point Unit 2 (NMP2) steam dryer for operation at Extended Power Uprate (EPU). The stress analysis methodology used for this evaluation does not consider the presence of cracking in the steam dryer structure; however, several reportable indications were identified while performing an in-vessel visual inspection (IVVI) of the Nine Mile Point Unit 2 (NMP2) steam dryer [1] during the Spring 2008, RF011 outage. The indications were observed in the upper support ring, the drain channel to skirt vertical weld, and in the tie bar to hood weld heat affected zone (HAZ).

CDI has subsequently contracted with Structural Integrity Associates (SI) to perform the following:

1. Fracture mechanics evaluation of observed indications to determine likelihood for further crack growth and potential for generation of loose parts or loss of ability of the steam dryer to perform its design function. The output of this work will help determine if repairs are required for any of the indications.
2. Vibration assessment of observed indications to determine what effect the observed cracking will have on the dynamic characteristics of the steam dryer. The output of this work will help determine if cracking must be considered in the EPU stress analysis for the Nine Mile Point Unit 2 (NMP2) steam dryer.

The fracture mechanics evaluation is discussed first followed by the vibration assessment. Each component (upper support ring, drain channel, and tie bars) are discussed separately.

2.0 OBSERVED CRACKING

The BWRVIP-139 [4] and SIL 644 [15] inspections documented in Reference [1] have identified steam dryer indications in the following components:

- Drain Channels
- Upper Support Ring
- Tie Bar attachment welds
- Vane Bank tie rod cam nut tack welds
- Lifting rod to lug tack welds

This evaluation considers the indications in the drain channel, upper support ring and tie bar attachment welds. The cam nut tack welds and the lifting rod lug tack welds have no impact on the steam dryer structural response as these a non structural welds. These tack welds are locking devices and will be addressed with repair measures.

The upper support ring cracking is documented in Indication Notification Form 08-24 (INF 08-24) of Reference [1]. This form identifies 89 reportable indications distributed around the circumference of the upper support ring. The majority of the indications are located at the lower corner of the outer surface of the ring; however, approximately 3 indications (#55, #56, #57 from INF-08-24 [1]) are seen to initiate at the upper corner of the outer surface. Four (4) indications are oriented horizontally (#9, #13, #55, #56 from INF-08-24 [1]); whereas, the remaining 85 indications are vertical. Although the INF does not report a horizontal dimension for any of the horizontal indications, the bounding horizontal indication length is given by Constellation Energy Group as 10 inches [2]. The vertical indications can be sized from the images contained in the INF. The bounding dimension for the vertical indications is 1 inch. Because the indications were identified during IVVI, no depth dimension could be determined; all dimensions are considered to be lengths. Table 2-1 summarizes the bounding indication lengths considered for this evaluation. Considering the large number of cracks in the upper support ring, photographs of each indication are not provided in this report; however, for information, representative photographs are contained as Figures 2-1 and 2-2.

INF-08-21 [1] identifies two reportable indications, E and H, in the Drain Channel weld DC-V3-320. INF-08-22 [1] identifies one reportable indication, G, in the Drain Channel weld DC-V7-

140. All three indications are located in the vertical weld joining the 1/8" drain channel to the ¼" skirt and are oriented approximately perpendicular to the weld. The right ends of each indication appear to stop at the weld and the left ends are in the skirt material. There are no signs that these indications are propagating into the drain channel material or through the weld. The lengths of indications E, H, and G, respectively, are reported as 1.61, 1.64, and 0.67 inches. The INFs also report the length from the previous inspection from which an apparent growth can be determined. Table 2-1 summarizes the 2008 indication lengths considered for this evaluation. Table 2-2 summarizes the apparent crack growth for each indication over the previous operational cycle. Figures 2-3 through 2-5 show inspection photographs of the drain channel indications.

Also note that although the 2008 IVVI report [1] does not identify cracking in the tie bar attachment welds, Constellation Energy Group has requested that the Tie Bar cracking previously identified be evaluated with respect to EPU operation. Figures 2-6 through 2-7 are representative photographs of the tie bar cracking provided by Constellation Energy Group [3].

Table 2-1. Summary of Indication Dimensions Considered in Evaluation.

Location	Orientation	2008 Dimension, in	Note
Upper Support Ring	Horizontal	10	Bounding value provided by Constellation Energy Group [2]
Upper Support Ring	Vertical	1	Bounding value taken from INF-08-24 [1]
DC-V3-320	Perpendicular to vertical weld	1.61	Indication E in INF-08-21 [1]
DC-V3-320	Perpendicular to vertical weld	1.64	Indication H in INF-08-21 [1]
DC-V7-140	Perpendicular to vertical weld	0.67	Indication E in INF-08-22 [1]

Table 2-2. Apparent 1-cycle Crack Growth for Drain Channel Indications.

Location	2006 Dimension, in	2008 Dimension, in	Apparent Crack Growth, in
DC-V3-320 Indication E	1.17	1.61	0.44
DC-V3-320 Indication H	1.44	1.64	0.2
DC-V7-140 Indication G	0.49	0.67	0.18

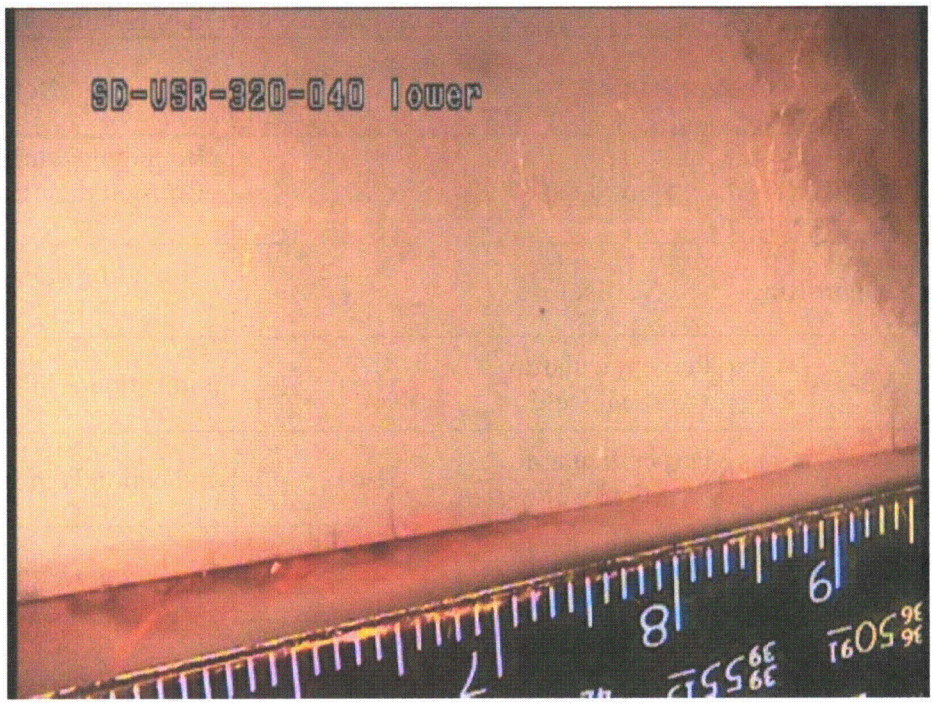

Figure 2-1. Representative Photograph of Vertical Indications in Upper Support Ring.

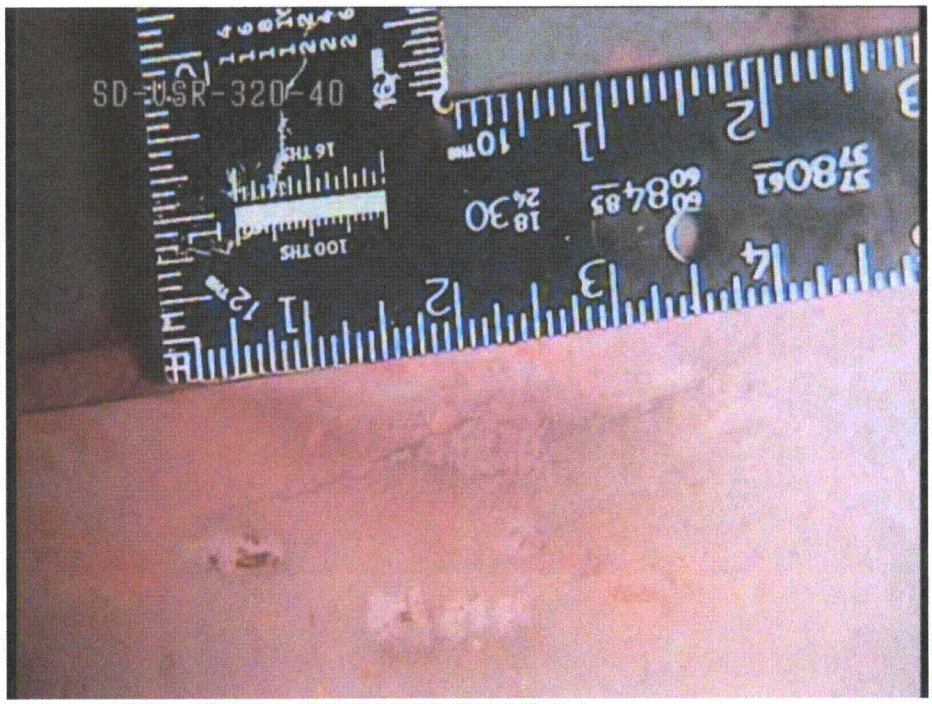

Figure 2-2. Representative Photograph of Horizontal Indications in Upper Support Ring.

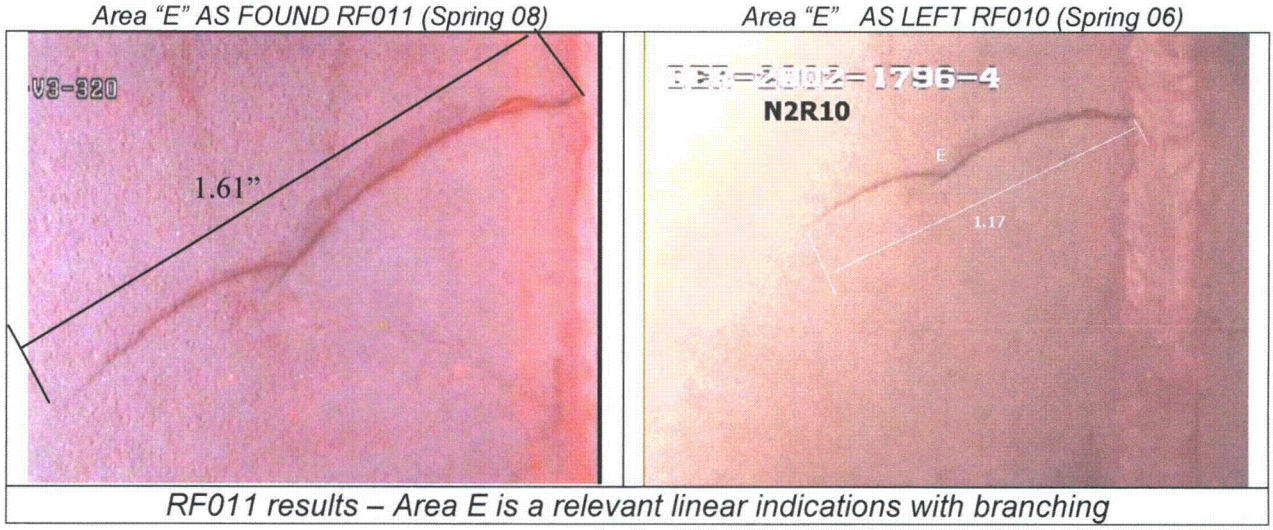

Figure 2-3. INF-08-21 Photograph of DC-V3-320 Indication E [1].

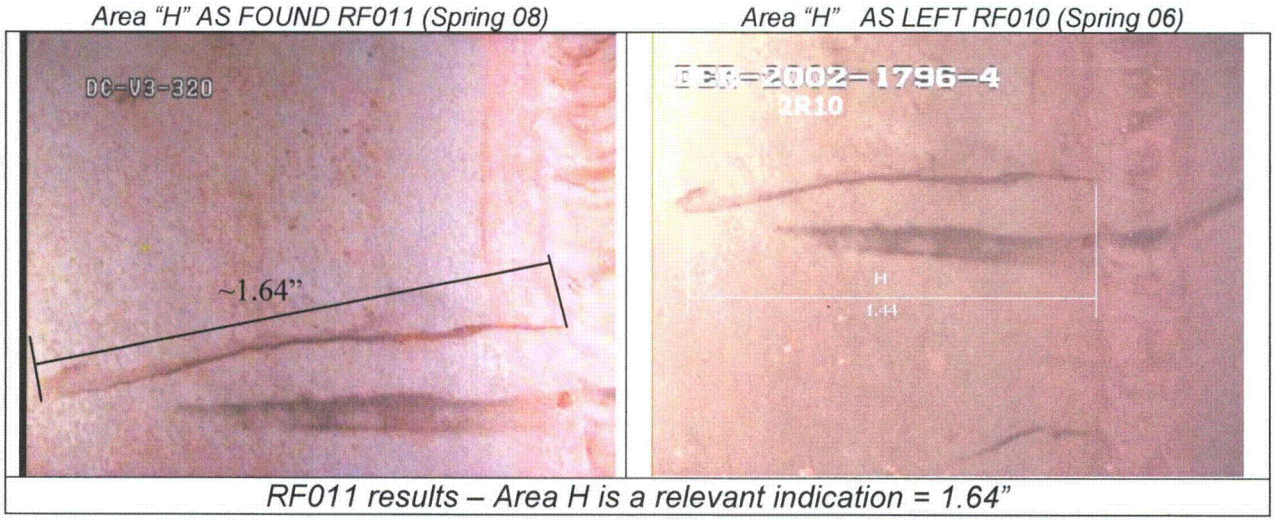

Figure 2-4. INF-08-21 Photograph of DC-V3-320 Indication H [1].

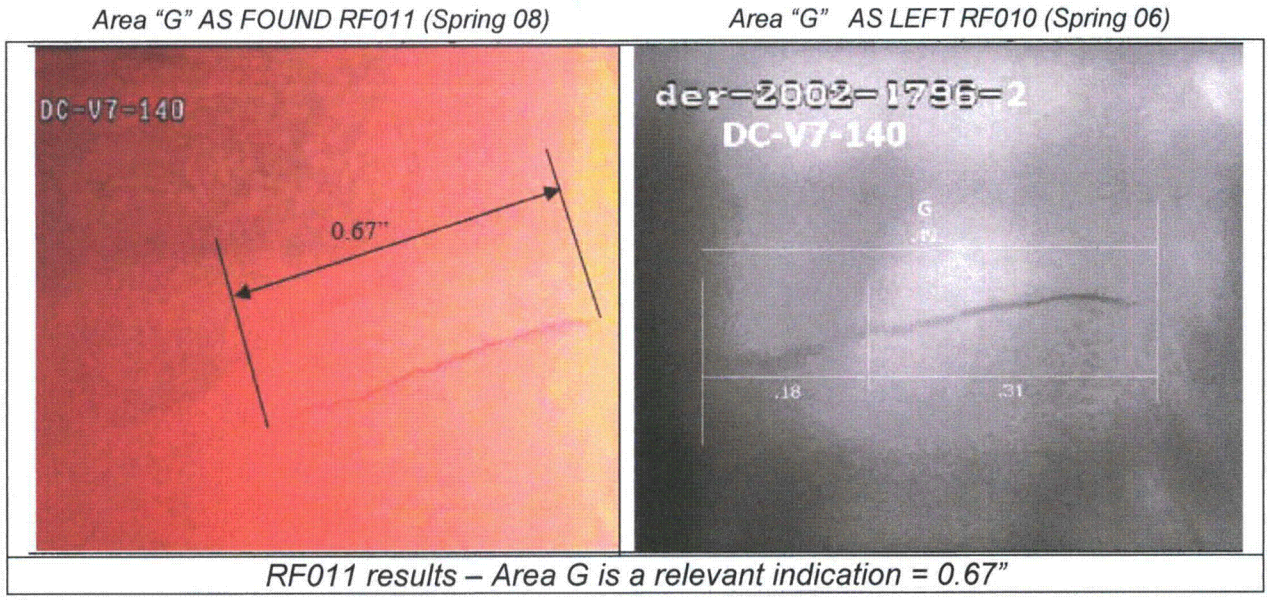

Figure 2-5. INF-08-22 Photograph of DC-V7-140 Indication G [1].

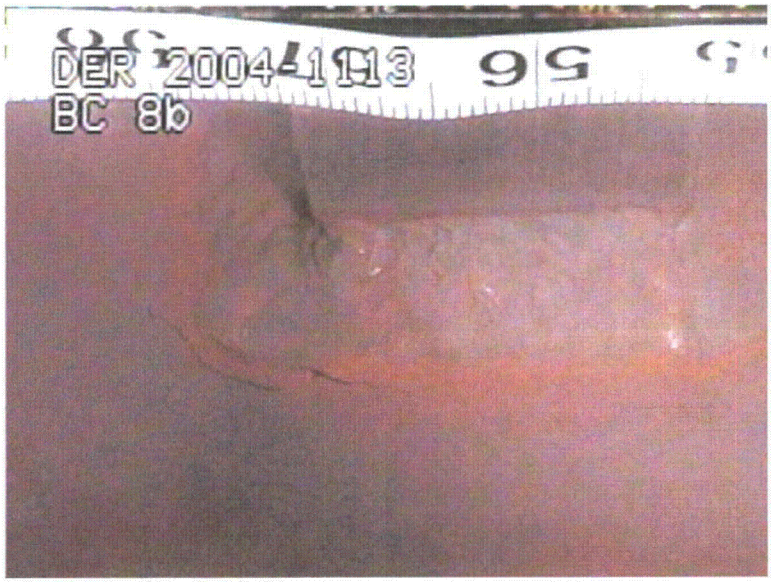

Figure 2-6. Representative Photograph of Tie Bar Cracking.

Figure 2-7. Representative Photograph of Tie Bar Cracking.

3.0 INPUT DATA

This section summarizes the input data used to characterize the problem. Input is summarized for each component addressed in this report (Upper Support Ring, Drain Channel, Tie Bar)

3.1 Upper Support Ring Input Data

The following inputs are used to characterize the problem:

- Geometry
- Material
- Location and nature of boundary conditions
- Extent of observed cracking (See Section 2.0)

3.1.1 Upper Support Ring Geometry

The upper support ring is a 3.5 inch by 9.5 inch (width x height) rectangular type 304 stainless steel member [6]. The upper support rings are generally cut from annealed plate then cold formed into the ring [4]. Two half rings are spliced together with a bolted splice plate to form the entire circumference of the upper support ring [4]. This component rests on top of the dryer support brackets welded to the Reactor Pressure Vessel (RPV) wall. This component is a structural member to which the skirt and outer hoods are attached. The radius of curvature of the inside surface of the ring is 119.5 inches [6]. Figure 3-1 illustrates the general location of the Upper Support Ring in the steam dryer assembly.

3.1.2 Upper Support Ring Material

The upper support ring is Type 304 stainless steel plate with the following material properties:

- Elastic Modulus, E, at 550 °F = 25.5E6 psi
- Poisson's Ratio, ν, = 0.3
- Density, ρ, = 0.283 lb/in^3

3.1.3 Upper Support Ring Boundary Conditions

The upper support ring rests on four steam dryer support brackets evenly spaced around the RPV inner diameter. The supports are rectangular brackets welded to the RPV. The azimuthal locations of the brackets are 4°, 94°, 184°, and 274° [6]. The dryer skirt is welded to the upper support ring with a single sided fillet weld at the bottom of the ring. The outer hoods are welded to the top of the upper support ring with single sided fillet welds as well.

3.2 Drain Channel Vertical Weld Input Data

The following inputs are used to characterize the problem:

- Geometry
- Material
- Location and nature of boundary conditions
- Extent of observed cracking (See Section 2.0)

3.2.1 Drain Channel & Skirt Geometry

The steam dryer skirt is a ¼" thick shell with a radius of curvature of ~119 inches [6]. The height of the skirt and drain channel from the weld at the base of the upper support ring to the free end at the bottom of the steam dryer is ~92 inches [6]. The cracking observed adjacent to the drain channel weld occurs in the skirt shell between the drain channels. The width of the gap between the drain channels is 23" [6]. Figure 3-1 provides a general schematic of the geometry.

3.2.2 Drain Channel & Skirt Material

The dryer skirt and drain channel are Type 304 stainless steel plate with the following material properties:

- Elastic Modulus, E, at 550 °F = 25.5E6 psi
- Poisson's Ratio, ν, = 0.3
- Density, ρ, = 0.283 lb/in^3

3.2.3 Drain Channel & Skirt Boundary Conditions

The drain channel and skirt are welded to the base of the upper support ring at the top of the skirt and drain channel plates. The bottom 30" of the drain channel and skirt are submerged in reactor coolant. The drain channel plate is welded to the skirt to form the drain channel enclosure. A lower ring forging is welded to the skirt at the base of the skirt.

3.3 Tie Bar Input Data

The following inputs are used to characterize the problem:

- Geometry
- Material
- Location and nature of boundary conditions
- Extent of observed cracking (See Section 2.0)

3.3.1 Tie Bar Geometry

The tie bar is a structural member of rectangular cross-section designed to provide support between the top hoods of adjacent dryer vane banks. This component helps to retain the dryer shape and is attached to the top hood with fillet welds. Figure 3-2 identifies the tie bar locations considered in this evaluation and illustrates the general location of the tie bars on the steam dryer assembly.

3.3.2 Tie Bar Material

The tie bar and top hoods on the dryer are Type 304 Stainless Steel. The attachment welds are most likely applied with ER308 weld material.

3.3.3 Tie Bar Boundary Conditions

For this evaluation the tie bar is considered a rigid member, rigidly attached to a plate with pinned boundary conditions.

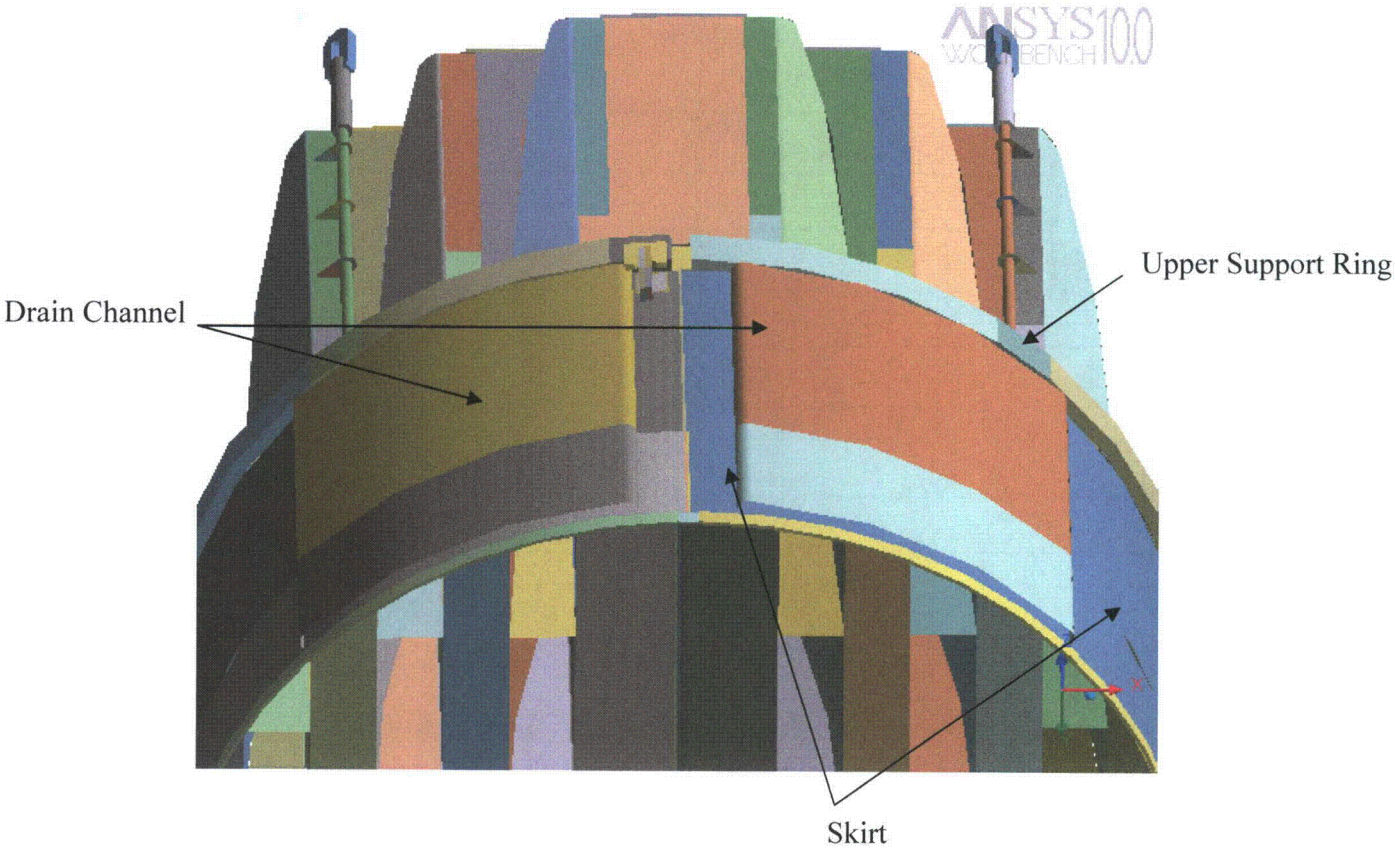

Figure 3-1. NMP2 Steam Dryer Model Showing Upper Support Ring, Drain Channel, and Skirt.

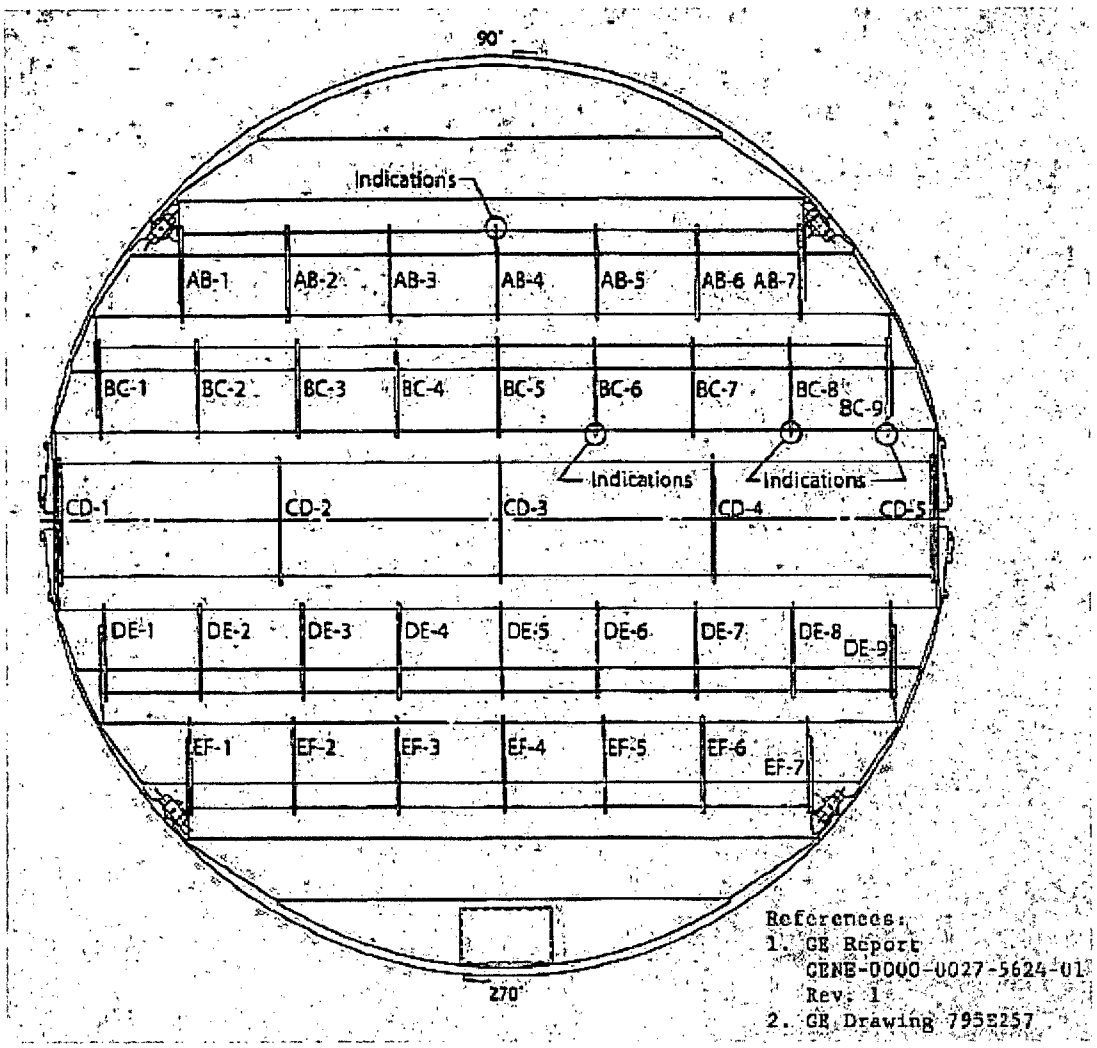

Figure 3-2. Orientation of Tie Bars on Steam Dryer Assembly [4].

4.0 FLAW EVALUATION

This section individually documents flaw evaluations performed for the indications observed in the NMP2 steam dryer. The results of these evaluations will be used to perform the vibration assessment of the cracked steam dryer components in Section 5.0.

4.1 Upper Support Ring

This section describes the evaluation performed for the steam dryer upper support ring. Conservative methods are used to determine a bounding assessment of the expected crack growth.

4.1.1 Assumptions

The following assumptions are used to augment the analysis methods described below:

1. Upper support ring cracking has been observed in other plants; this cracking has typically been attributed to IGSCC driven by the residual stresses induced in the material during the cold forming process.
2. The radius of curvature to ring thickness ratio, R/t, is sufficiently large that the upper support ring can be treated as a straight beam rather than a ring.
3. The vertical indications in the upper support ring can be modeled as corner cracks in a plate or bar.
4. An aspect ratio, a/c, of 1.0 is assumed for all vertical indications.
5. The horizontal indications in the upper support ring can be conservatively modeled as through wall cracks in an infinite plate.
6. The mode I stress intensity factor, K_I, is expected to be small; therefore, a plastic zone size correction is not included in the linear elastic fracture mechanics (LEFM) solution.
7. The alternating stress intensity factor used for calculation of fatigue crack growth (FCG), ΔK_I, is obtained from the range of alternating stress intensity contributed by flow induced vibration (FIV) loading only.
8. System thermal cycles, seismic and hydraulic loads contribute an insignificant number of cycles during the next operating period; therefore, they make a negligible contribution to FCG compared to FIV loading and are not calculated here.

9. Deadweight, steady state thermal loads, differential pressure, and weld residual stresses contribute to the mean K_I rather than ΔK_I; therefore, they are considered only in the selection of a conservative R-ratio and not specifically considered in calculation of a mean K_I. Assuming an R-ratio of 1 incorporates the maximum effects of mean stress on the expected FCG of the steam dryer indications.

4.1.2 Methods

The fracture mechanics evaluation of the upper support ring indications is performed using the following methods:

1. FIV stresses at EPU conditions are obtained from the uncracked finite element model (FEM) as provided by CDI [6].
2. The maximum stress intensity obtained from all locations through the ring thickness and around the entire circumference of the ring is assumed to act as a membrane stress on the each crack face. This conservatively applies the maximum stress to all indications.
3. Each indication is treated separately. Closely spaced flaws will experience a reduction in driving force caused by an effective "shielding" of the flaws; treating them as single flaws, remote from other flaws, maximizes the calculated K_I.
4. Both FCG and Stress Corrosion Crack Growth (SCC) are evaluated separately which is consistent with the methods of ASME BP&V Code, Section XI [7].
    a. The expected FCG growth is determined using the methods contained in Article C-3000 of the ASME B&PV Code, Section XI [7].
    b. The expected SCC crack growth for each indication is calculated assuming a 100% capacity factor, a two year fuel cycle, and the accepted bounding IGSCC growth rate of 5×10^{-5} in/hr per crack tip.
5. For the vertical indications the K_I solution given by Raju and Newman for a corner cracked plate subjected to a membrane load is used [8].
6. For the horizontal indications a center cracked panel solution for a uniform membrane stress distribution is used [9].

4.1.3 Results

Recognizing that the flaws observed in this component are attributed to IGSCC, a crack growth contribution from IGSCC is calculated for the next operational cycle and given below as:

$$\Delta a_{IGSCC} = 2yr \cdot 365.25\frac{days}{yr} \cdot 24\frac{hr}{day} \cdot 5x10^{-5}\frac{in}{hr} = 0.877\frac{in}{flaw_tip}$$

Vertical Indications

From Table 2-1 the bounding vertical indication dimension is 1 inch. This flaw dimension is increased by the predicted SCC crack growth over the next cycle to calculate a bounding ΔK_I for a FCG calculation. The flaw aspect ratio is kept constant at 1; therefore, the corner crack dimension evaluated for FCG is 1.877 inch. Raju and Newman [8] give the Mode I stress intensity solution for a corner cracked plate at any angle along the crack front to be:

$$K_I = \sigma F\sqrt{\pi\frac{a}{Q}} \qquad (1)$$

Where: σ is a uniform stress distribution, psi

a is the crack depth measured through the plate thickness, in

Q is the shape factor for an ellipse given by the complete elliptic integral of the second kind.

F is the boundary correction factor given by equations or taken from tables in [8].

The maximum stress intensity at any location in the upper support ring is given by CDI [6] as 343 psi. This stress intensity is conservatively assumed to be the maximum principal stress acting normal to the crack face, uniform across the thickness of the ring and constant around the entire circumference of the ring. Then, the resulting range of K_I considered for FCG is obtained from:

a/c=1

a=1.877

a/t=1.877/3.5=0.54

σ=0.343 ksi

Q=2.464 (See page I-242 of [8])

F=1.30 (Bounding value for a/c=1 interpolated from a/t=0.5 and a/t=0.8, see page I-244 of [8])

ΔK_I=0.69 ksi-in$^{0.5}$

Horizontal Indications

From Table 2-1 the bounding horizontal indication dimension is 10 inches. This flaw dimension is increased by the predicted IGSCC crack growth at each crack tip over the next cycle to calculate a bounding ΔK_I for a FCG crack growth calculation. The flaw dimension evaluated for FCG is 11.75 inches. Reference [9] gives the Mode I stress intensity solution for a center cracked panel, assuming the width of the panel is much greater than a, as:

$$K_I = \sigma\sqrt{\pi a} \qquad (2)$$

Where: σ is a uniform stress distribution, psi

a is the crack half length, in

The maximum stress intensity at any location in the upper support ring is given by CDI [6] as 343 psi. This stress intensity is conservatively assumed to be the maximum principal stress acting normal to the crack face, uniform across the thickness of the ring and constant around the entire circumference of the ring. Then, the resulting range of K_I considered for FCG is obtained from:

a=5.877

σ=0.343 ksi

ΔK_I=1.47 ksi-in$^{0.5}$

Table 4-1 summarizes the maximum range of alternating stress intensity and ΔK_I for the vertical and horizontal indications in the Upper Support Ring. Review of the FCG growth correlations for Austenitic stainless steel in an air environment given in Figure C-8410-1 [7], contained in this report as Figure 4-1, shows that, for an R ratio of 0.9 (the largest given in this figure), a very small incremental fatigue crack growth is expected for a $\Delta K_I < 3$ ksi-in$^{0.5}$.

Neither the vertical nor horizontal indications are expected to exhibit significant growth from fatigue or SCC such that the upper support ring creates loose parts or inhibits the steam dryer assembly from performing its design function. This assessment is supported by the substantial field experience from the operating fleet in which upper support ring cracking has existed for many years without exhibiting continuous growth. The field experience supports the judgment that the flaws are IGSCC initiated by the high residual stresses on the OD of the support ring induced from the cold forming process used to fabricate the sections. These residual stresses are relieved as the crack is formed and do not drive further growth. FCG is shown to be negligible considering the low range of alternating stresses in the upper support ring.

4.2 Drain Channel

This section describes the flaw evaluation of the indications in the drain channel vertical welds. Conservative methods are used to determine a bounding assessment of the expected crack growth.

4.2.1 Assumptions

The following assumptions are used for the subject flaw evaluation:

1. The flaw exists in the base metal and is oriented perpendicular to the weld and HAZ; therefore, it has the characteristics of a fatigue crack.
2. The flaw configuration can be modeled as a center crack in an infinite plate.
3. The mode I stress intensity factor, K_I, is expected to be small; therefore, a plastic zone size correction is not included in the LEFM solution.
4. The alternating stress intensity factor used for calculation of FCG, ΔK_I, is obtained from the range of alternating stress intensity contributed by FIV loading only.

5. The subject geometry is a thin plate; therefore, the stress state will be characterized by a plane stress condition. This will result in one of the three principal stresses being close to zero. In this case it is conservative to assume the crack driving force is bounded by the ASME B&PV Code defined stress intensity acting as a membrane stress along the entire surface of the crack face. The stress intensity will always be equal or larger to the largest principal stress component for this configuration. Further, for plates, the through-wall stress distribution will exhibit tensile stresses on one side and compressive stresses on the opposite side. This stress distribution suggests that the flaw would likely not grow through-wall.
6. System thermal cycles, seismic and hydraulic loads contribute an insignificant number of cycles during the next operating period; therefore, they make a negligible contribution to FCG compared to FIV loading and are not calculated here.
7. Deadweight, steady state thermal loads, differential pressure, and weld residual stresses contribute to the mean K_I rather than ΔK_I; therefore, they are considered only in the selection of a conservative R-ratio and not specifically considered in calculation of a mean K_I. Assuming an R-ratio of 1 incorporates the maximum effects of mean stress on the expected FCG of the steam dryer indications.

4.2.2 Methods

The fracture mechanics evaluation of the drain channel indications is performed using the following methods:

1. The EPU FIV range of alternating stress intensities output from the existing uncracked FEM of the NMP2 steam dryer for a region spanning the length of the vertical weld by 7 inches wide across the weld are reviewed. A bounding range of alternating stress intensity is selected.
2. The bounding range of alternating stress intensity is conservatively scaled by a weld factor of 1.8 to incorporate peak stress effects.
3. The range of stress intensity factor experienced as a result of the EPU FIV loading is calculated using a center cracked panel solution for a uniform membrane stress distribution [9].

4. The FCG expected during the next operational cycle is determined using the methods contained in Article C-3000 of the ASME B&PV Code, Section XI [7]. Note that since the flaw exists in the base metal and is not considered to be IGSCC, no SCC growth must be calculated.

4.2.3 Results

From Table 2-1 the bounding indication dimension from welds DC-V3-320 and DC-V7-140 is 1.64 inches. From Table 2-2, the bounding apparent crack growth for all indications was 0.44 inches. The conservative flaw dimension used to calculate expected FCG over the next cycle is taken as 2.08 inches. Reference [9] gives the Mode I stress intensity solution for a center cracked panel, assuming the width of the pane is much larger than a, as:

$$K_I = \sigma\sqrt{\pi a} \qquad (2)$$

Where: σ is a uniform stress distribution, ksi
a is the crack half length, in

Figure 4-2 shows the EPU FIV stress intensity distribution along the length of weld DC-V3-320 [6]. In this figure, the portions of the skirt and drain channel above and below water are identified. Figure 4-3 shows the EPU FIV stress intensity distribution along the length of weld DC-V3-320 and at the edges of the 7" region adjacent to and approximately centered over the vertical weld. These figures show that the maximum stress intensity of ~800 psi occurs toward the bottom of the vertical weld and attenuates to ~200 psi up the length of the weld. The stress intensity is also shown to attenuate rapidly away from the submerged portion of the skirt but remain relatively constant above the water level. The approximate vertical locations of each of the three indications in the DC-V3-320 and DC-V7-140 welds are also identified on Figure 4-3 [2]. The stress distribution from the DC-V3-320 weld is used for the DC-V7-140 weld as well. Table 4-2 summarizes the maximum stress intensity along the vertical weld for the skirt and drain channel both above and below the water level.

Although there is no evidence that the indications in the drain channel vertical welds are actually in the drain channel and none of the indications are at the location of maximum stress, the flaw evaluation is performed using both the bounding stress from the region applied as a uniform membrane stress and using a more representative stress from the skirt material applied as a uniform membrane stress. Then the resulting range of K_I considered for FCG is obtained from:

a=1.04 inches

$\sigma_{drain\ channel}$=0.846 ksi

Weld Factor = 1.8

ΔK_I=2.75 ksi-in$^{0.5}$

a=1.04 inches

σ_{skirt}=0.215 ksi

Weld Factor = 1.8

ΔK_I=0.70 ksi-in$^{0.5}$

Note that these results are very conservative in that they take no credit for the rapid attenuation of stresses in the drain channel as the crack grows away from the weld. Rather the peak stress is assumed to remain at the peak value and be uniform across the entire crack face as the crack grows deeper into the skirt away from the weld. Further, for both the drain channel and skirt calculation the weld factor of 1.8 is applied to further increase the stresses. This conservatively assumes that the peak stress effects which are confined to a local region at the weld root are applied across the entire crack face regardless of crack size.

Table 4-1 summarizes the maximum range of alternating stress intensity and ΔK_I for the drain channel indications. Review of the FCG correlations for austenitic stainless steel in an air environment given in Figure C-8410-1 [7], contained in this report as Figure 4-1, shows that, for an R ratio of 0.9 (the largest given in this figure), a very small incremental fatigue crack growth is expected for a $\Delta K_I < 3$ ksi-in$^{0.5}$.

These results show that regardless of where an indication exists along the length of the drain channel vertical weld and regardless of whether it occurs in the drain channel or skirt, the expected FCG is minimal.

The drain channel indications are not expected to create loose parts or inhibit the steam dryer assembly from performing its design function. This assessment is supported by the substantial field experience from the operating fleet in which drain channel cracking has existed for many years without causing significant failures of steam dryer components.

4.3 Tie Bars

The IGSCC indications observed in four of 37 tie bars on the NMP2 steam dryer have previously been evaluated and shown to be acceptable for operation at Current Licensed Thermal Power (CLTP) [10]. These indications have been observed since RF09 (2004) and have been monitored during each refueling outage without any observed crack growth [2]. The location and structure of the indications are indicative of IGSCC initiated as a result of the high residual stresses caused by welding the Tie Bars to the dryer hoods. The indications are seen to remain in the HAZ and not propagate outside of this region. Further, all indications remain jagged and do not exhibit the characteristics of FCG. If FCG were a significant contribution to propagation of these flaws then growth would have been observed over the previous operating cycles. Even with the increase in steam dryer loads resulting from EPU operation the behavior of these flaws is not expected to change. Continual monitoring of these locations can confirm this assessment and identify if additional growth occurs in the future. The location and accessibility of these components makes repair of the locations possible if future conditions warrant. The current extent of cracking is small and is not expected to create loose parts or inhibit the design function of the steam dryer assembly.

Table 4-1. Summary of K_I results for NMP2 Steam Dryer Indications.

Location	Crack Dimensions, in	Stress, psi	K_I, Ksi-in$^{0.5}$
Upper Support Ring Vertical Indications	1.877 (Corner Crack)	343	0.69
Upper Support Ring Horizontal Indications	11.75 (Through wall)	343	1.47
Drain Channel	2.04 (Through wall)	846	2.75
Skirt	2.04 (Through wall)	215	0.70

Note: Dimensions listed in Table correspond to 2a for center cracked panel solutions.

Table 4-2. Summary of Maximum EPU FIV Stress Intensity Along Weld DC-V3-320.

Location	Max Stress, psi
Skirt	194
Submerged Skirt	215
Drain Channel	172
Submerged Drain Channel	846

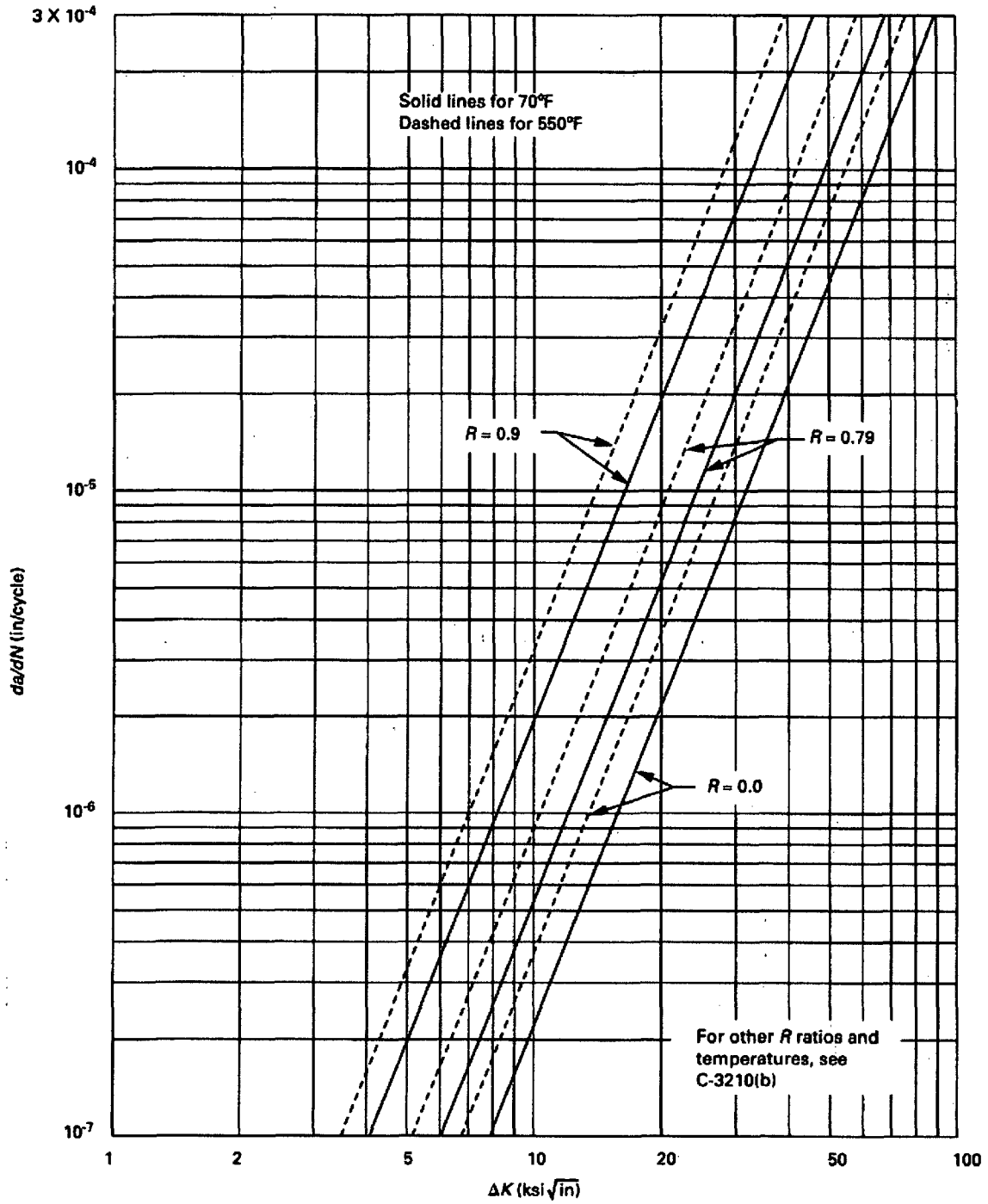

Figure 4-1. Reference Fatigue Crack Growth Curves for Austenitic Stainless Steels in Air Environments [Fig. C-8410-1, 7].

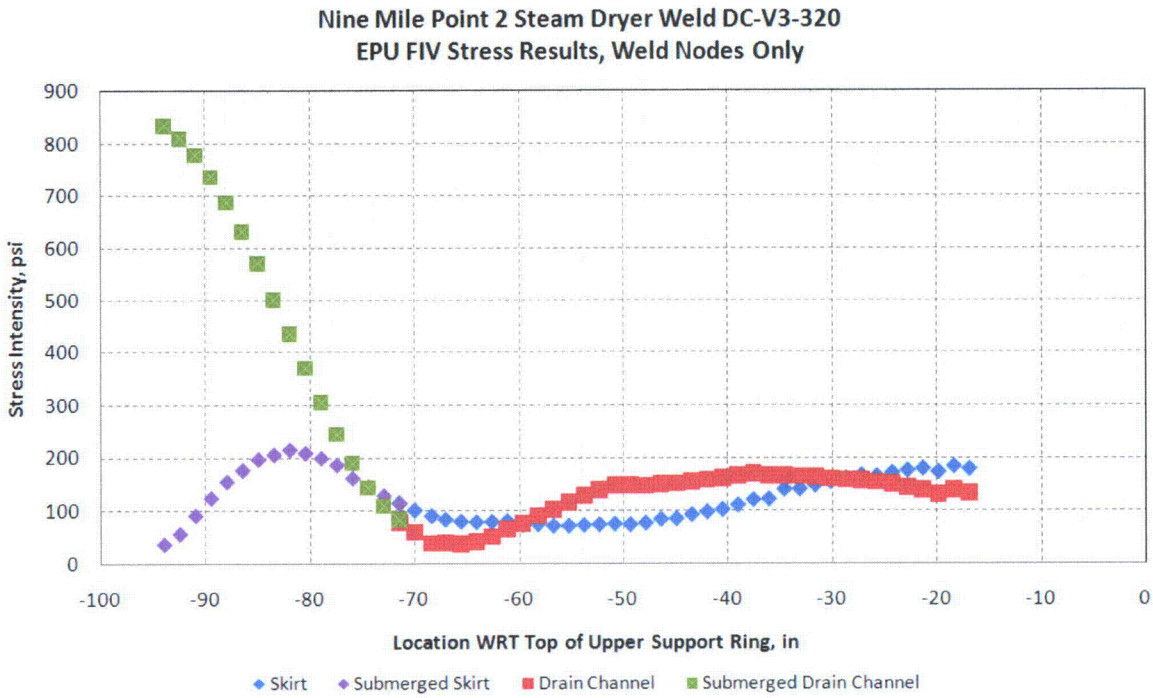

Figure 4-2. NMP2 EPU FIV Stress Intensity Along Weld DC-V3-320.

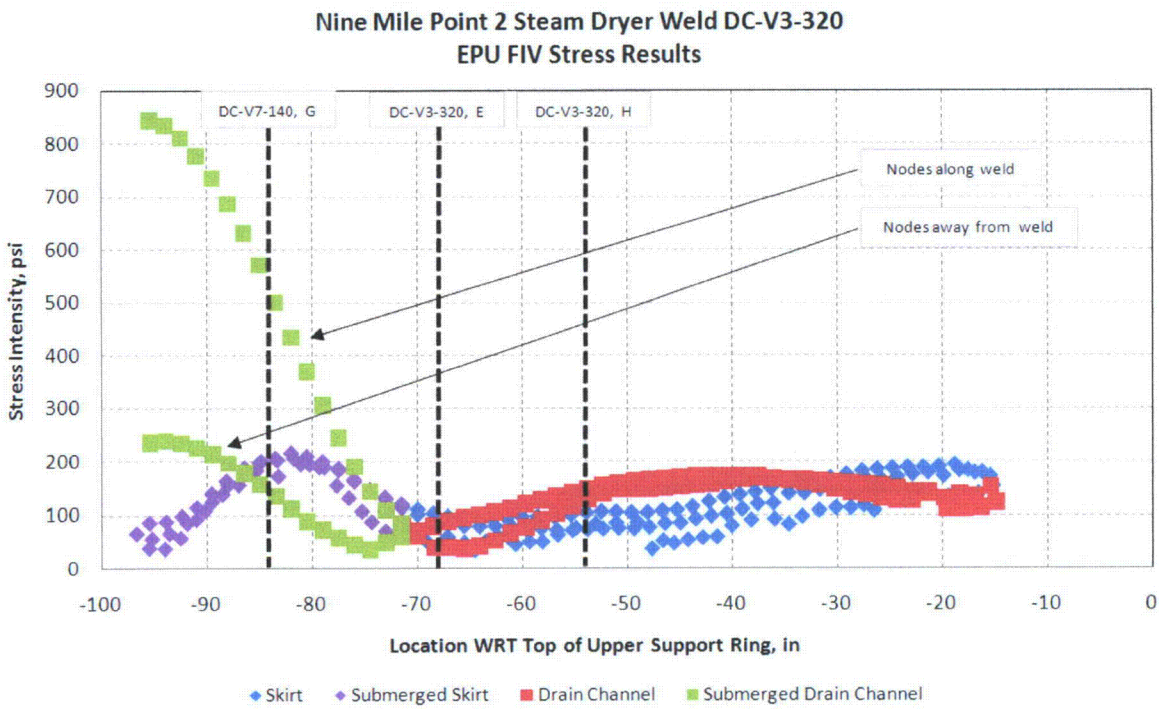

Figure 4-3. NMP2 EPU FIV Stress Intensity Along and Adjacent to Weld DC-V3-320.

5.0 VIBRATION ASSESSMENT

This section documents the vibration assessment performed for the upper support ring and the drain channels in the NMP2 steam dryer. Each component is addressed separately below.

5.1 Upper Support Ring

This section describes the evaluation performed for the steam dryer upper support ring. Conservative methods are used to assess the expected effect of cracking on the dynamic characteristics of this component.

5.1.1 Assumptions

The following assumptions are used to augment the analysis methods described below:

1. The upper support ring is treated as a straight beam of rectangular cross-section rather than a ring of rectangular cross-section. Curved beams for which the radius of curvature is in the plane of bending and for which the radius of curvature is at least ten times the beam depth are generally treated as straight beams [11]. The ratio of the radius of curvature to the beam width for the NMP2 upper support ring is 119.5/3.5 = 34.1; therefore, it is acceptable to treat the upper support ring as a straight beam for this evaluation.
2. Only the indications oriented vertically are considered in this evaluation. The circumferential indication is not oriented such that it will affect the stiffness of the support ring for either in plane or transverse vibration.
3. All vertical indications are assumed to be edge cracks extending across the entire outer surface of the upper support ring. This assumption is very conservative considering that the maximum length of all vertical cracks is conservatively predicted to be approximately 1.877" at the end of the next operating cycle; whereas, this assumption defines all cracks to be 9.5" long.
4. Each IGSCC indication is assumed to have an opening width, δ, of 0.010 inches. This value is consistent with typical assumptions used for fracture mechanics evaluations of IGSCC.

5. All 85 vertical indications are lumped together to form one indication of crack opening width equivalent to the sum of all indications. In other words a single notch is considered in this evaluation with a width of 85*0.01 = 0.85 inches. This equivalent notch is placed at the location of maximum moment in the beam model in order to maximize the reduction in stiffness. In a general case where multiple flaws are distributed throughout the beam length some would occur at areas of large moment, contributing greatly to the reduced stiffness, and others would occur at areas of small moment, contributing much less to the reduced stiffness. For this analysis all flaws are located such that they contribute the maximum amount towards a reduction in beam stiffness.

5.1.2 Methods

The effect of cracking on the dynamic characteristics of the upper support ring is estimated by evaluating the effect of a notch on the free vibration of a beam. Taking a straight beam of arbitrary cross-section and mechanical properties, using Euler-Bernoulli beam theory to characterize its behavior, letting external moments equal zero, and solving the equations of equilibrium gives the following partial differential equation for the transverse displacement of a beam in bending [12]:

$$-\frac{\partial^2}{\partial x^2}\left[E(x)\cdot I(x)\cdot\frac{\partial^2 y(x,t)}{\partial x^2}\right]=m(x)\cdot\frac{\partial^2 y(x,t)}{\partial t^2};\quad 0<x<L \qquad (3)$$

Equation (3) can be interpreted as the equivalence of a potential energy term given by the product of stiffness and displacement terms, and a kinetic energy term given by the product of mass and displacement terms. The solution of Equation (3) depends on the boundary and initial conditions defined for the beam. Generally, for beams of uniformly distributed parameters, where I(x), E(x), and m(x) are constant, exact solutions can be found. These solutions follow the same general approach briefly summarized below [12]:

1. Let free vibration be characterized by synchronous motion in the beam, then
2. The displacement solution is separable in the spatial and temporal terms,

$$y(x,t)=Y(x)\cdot G(t) \qquad (4)$$

3. This allows Eq. (3) to be reduced to the following form,

$$\frac{d^2}{dx^2}\left[E(x)\cdot I(x)\cdot\frac{d^2Y(x)}{dx^2}\right]=\omega^2 m(x)\cdot Y(x) \qquad (5)$$

4. The temporal term is assumed to take the form of $G(t)=C\cos(\omega t-\phi)$ (6)

Equation (5) is the differential eigenvalue problem. Notice that there is nothing inherently "dynamic" about the stiffness term; it is a function of the spatial variable only and can be analyzed from a static perspective. Stiffness is characteristic of the geometry and material and is applicable to both dynamic and static problems.

For our problem the material will be assumed to be uniform; therefore, E(x) is constant. Next, the effect of cracking on the dynamic characteristics of the upper support ring is estimated by evaluating the effect of a notch on the stiffness of a beam. Then, a reduced stiffness can be used to estimate a change in the natural modes of vibration caused by the cracking. Euler-Bernoulli beam theory is again used to derive equations for the static deflection shape of a beam. The presence of cracks in the beam is incorporated by defining an incremental length of beam with a section height reduced by the crack depth. In other words, the length of the cracked section is defined by the crack opening width of the crack and the cross-sectional area of the cracked section is given by the remaining ligament at the cracked section of the beam. The equations of beam deflection are solved for this beam model. Continuity is enforced at the junction between cracked and uncracked sections through the use of appropriate boundary conditions.

For uniform beams characterized by a length at least 10 times the depth, the displacement of a beam is governed by the applied moment and is described by [12]:

$$M(x)=E\cdot I\cdot\frac{d^2Y(x)}{dx^2} \qquad (7)$$

Consider the simple case of a fixed-free beam of constant cross-section supporting a static load applied at its free end. Solution of Equation (7) will require two boundary conditions. These

conditions are obtained by defining appropriate equations for the deflection or beam rotation at either boundary. Possible boundary conditions are:

$$Y(0) = 0 \tag{8a}$$

$$Y(L) = A \tag{8b}$$

$$\frac{dY(0)}{dx} = \theta(0) = 0 \tag{8c}$$

$$\frac{dY(L)}{dx} = \theta(L) = B \tag{8d}$$

Thus, for the simple case described above, the solution can be obtained from:

$$\frac{d^2Y(x)}{dx^2} = \frac{M(x)}{E \cdot I} \tag{9a}$$

$$Y(0) = 0 \tag{9b}$$

$$\frac{dY(0)}{dx} = \theta(0) = 0 \tag{9c}$$

Equation (9a) can be solved using the boundary conditions given in equations (9b) and (9c) to determine the constants of integration. The resulting equation for the displaced shape is:

$$Y(x) = \frac{P}{6EI}\left(x^3 - 3Lx^2\right) \tag{10}$$

Next, the displaced shape of a cracked beam can be determined using the same method but considering a composite beam formed of segments with different cross-sectional areas. Segments representing the cracked sections are defined by the cross-sectional area of the

remaining ligament at the cracked section. The uncracked segments are defined by the uncracked cross-sectional area of the beam. Any number of cracks can be considered by forming a composite beam composed of cracked and uncracked sections. The equation of the deformed shape will be piecewise continuous for each segment of the beam. The solution can be obtained by solving Equation (9a) with appropriate boundary conditions defined at the left and right boundaries of each section. The constants of integration for each section will be expressed as a function of the constants of integration from the previous section. For the case as defined by Assumption 5 the resulting beam problem is shown in Figure 5-1. This case is described by the following equations:

Section 1: Cracked Section at fixed boundary condition:

$$\frac{d^2Y_1(x)}{dx^2} = \frac{M(x)}{E \cdot I_1} \qquad \text{For } 0 \le x \le \delta \tag{11a}$$

$$Y_1(0) = 0 \tag{11b}$$

$$\frac{dY_1(0)}{dx} = \theta_1(0) = 0 \tag{11c}$$

Section 2: Uncracked Section:

$$\frac{d^2Y_2(x)}{dx^2} = \frac{M(x)}{E \cdot I_2} \qquad \text{For } \delta \le x \le L \tag{12a}$$

$$Y_2(\delta) = Y_1(\delta) \tag{12b}$$

$$\frac{dY_2(\delta)}{dx} = \frac{dY_1(\delta)}{dx} \tag{12c}$$

The solution to this problem can be shown to be:

$$Y_1(x) = \frac{P}{EI_1}\left(\frac{Lx^2}{2} - \frac{x^3}{6}\right) + C_{1,1}x + C_{1,2} \qquad \text{For } 0 \le x \le \delta \tag{13a}$$

$$C_{1,1} = C_{1,2} = 0 \tag{13b}$$

$$Y_2(x) = \frac{P}{EI_2}\left(\frac{Lx^2}{2} - \frac{x^3}{6}\right) + C_{2,1}x + C_{2,2} \qquad \text{For } \delta \le x \le L \tag{13c}$$

$$C_{2,1} = \frac{P}{E}\left(L\delta - \frac{\delta^2}{2}\right)\left(\frac{I_2 - I_1}{I_2 I_1}\right) \tag{13d}$$

$$C_{2,2} = \frac{P}{E}\left(\frac{\delta^3}{3} - \frac{L\delta^2}{2}\right)\left(\frac{I_2 - I_1}{I_2 I_1}\right) \tag{13e}$$

Although the presence of cracking changes the moment of inertia at the cracked section it can also be expressed as an equivalent Modulus of Elasticity for a beam keeping the moment of inertia constant. This approach is convenient if explicitly including cracks in an analytical solution is laborious. Comparison of the maximum deflection for the cracked case to the maximum deflection for the uncracked case can be expressed as an equivalent modulus of elasticity for an uncracked beam of constant cross-section. The effect of various crack depth to beam thickness ratios, a/W, as well as different equivalent crack opening width to beam length ratios, δ/L, are evaluated to assess the sensitivity of the upper support ring to cracking. A modified Elastic Modulus is calculated parametrically for:

a/W = [0.075,0.600]

δ/L = [0.00001,1]

From these results the effect of different crack sizes and numbers of cracks on the global stiffness of a simple beam model can be estimated. The term global is used because this approach effectively distributes the effect of the crack along the length of an uncracked beam such that the cracked beam and equivalent uncracked beam exhibit the same maximum deflection. The beam models are equivalent only at the boundaries and location of maximum deflection. The approximation of the effect that cracking has on the deflection of the beam allows us to investigate the effect on the beam stiffness, which as seen in Eq. (5), is necessary to assess the effect on the natural frequencies of a cracked beam.

Finally, it is noted that the natural frequencies of a beam are given in Reference [13] as:

$$f_i = \frac{\lambda_i^2}{2\pi L^2}\left(\frac{EI}{m}\right)^{0.5} \tag{14}$$

The values for λ vary depending on mode number and boundary conditions of the beam. The mode shape is given by transcendental equations independent of material or geometry. It can be seen that Eq. (14) is applicable to all modes. It is noted that for the cracked case, where cracking constitutes a small percentage of the beam length, the total length, L, the beam mass, m, and the Modulus of Elasticity, E, can be assumed invariant. Cracking effectively changes the moment of inertia at the crack location. As discussed above, it is possible to assume a constant moment of inertia along the beam length and express the effect of cracking as a modified elastic modulus; hence, the effect of cracking on the dynamic characteristics of the beam can be estimated by modifying the elastic modulus of the beam in Equation (14).

Recognizing that the approach used to estimate a cracked structure's natural frequency based upon an equivalent uncracked structure's dynamic characteristics is tied to a method which assumes uniformly distributed properties, it is judged prudent to limit use of this approach to notched sections less than or equal to 5% of the total beam length.

5.1.3 Results

The results of the parametric cases identified above are presented in Figures 5-2 and 5-3. Table 5-1 summarizes the constants of integration, incremental deflections for the cracked and uncracked beam segments, total deflection, and the equivalent elastic moduli for all parametric cases.

The following results are obtained for the specific case of the NMP2 upper support ring cracking:

1. To determine an a/W ratio applicable for NMP2, the area of the largest crack face is calculated as:

$$A_{corner} = \frac{\pi a_{corner}^{2}}{4} = 2.77 \text{ in}^2$$

   where the vertical cracks are assumed to be quarter circular cracks of length, a. Recall that the largest vertical cracks exhibited a length of ~1.877 inches after one cycle of SCC growth and FCG was shown to be insignificant.

2. An equivalent edge crack depth is calculated by forcing the crack face areas of the edge and corner cracks to be equivalent:

$$a_{edge} = \frac{A_{corner}}{H} = \frac{2.77}{9.5} = 0.292 \text{ in.}$$

3. The a/W for the edge crack is determined by:

$$\frac{a_{edge}}{W} = \frac{A_{corner}}{WH} = \frac{2.77}{(3.5)9.5} = 0.083$$

4. As stated in Assumption 5, for the 85 corner cracks observed in the NMP2 upper support ring an equivalent lumped crack opening width δ=0.85 inches is considered.

5. Recall that the equivalent modulus was defined using the static deflection shape of a fixed-free beam where the effect of all cracks was accumulated at the location of maximum moment. The characteristic length used for this evaluation should be defined consistent with the approach used to determine the effective modulus. Approximating the fundamental mode of the ring in transverse vibration by a fixed free beam of characteristic length defined by the distance between adjacent support blocks gives a length of:

$$L = \frac{2\pi R}{4} = \frac{119.5 \cdot \pi}{4} = 94 \text{ in.}$$

This length is chosen since the vibration mode will be symmetric about a line assumed to occur between two support blocks diametrically opposite each other and will exhibit maximum displacement at the other two support blocks. Since the beam is not clamped to the blocks this mode will not be restrained. This is considered to be the shortest length that can be defined using assumptions consistent with the manner in which the modified elastic modulus was obtained.

6. This results in a $\delta/L=0.009$, which corresponds to an equivalent notched length less than 1% of the total beam length and is within the assumed limits of the approximate methods used here.

7. From Figures 5-2 and 5-3, using a $\delta/L=0.009$, and interpolating between an $a/W=0.075$ and an $a/W=0.150$, a ratio of effective elastic modulus to uncracked elastic modulus of approximately 0.99 is obtained.

8. From equation (14) the effect of the observed cracking on the natural frequencies of the upper support ring can be conservatively estimated to be a reduction in the uncracked natural frequencies of less than 0.5%. For cracking this minor the effect of cracking on the mode shapes is also expected to be negligible.

5.2 Drain Channel Vertical Weld

This section describes the evaluation performed for the steam dryer drain channel vertical weld. Conservative methods are used to assess the expected effect of cracking on the dynamic characteristics of this component.

5.2.1 Assumptions

The following assumptions are used to augment the analysis methods described below:

1. The drain channel and skirt are treated as flat plates for the purposes of evaluating the effect of cracking on the vibration characteristics of a panel.
2. The boundary conditions assumed for the skirt plate between the drain channels are:
    a. Clamped at the skirt to upper support ring weld
    b. Pinned at the skirt to drain channel welds
    c. Free at the base of the skirt
3. The effect of hydrodynamic mass on the submerged portion of the drain channel and skirt shell is neglected in this evaluation. It is not the intent of this analysis to determine the actual natural frequency of the cracked component; rather, it is desired to assess whether cracking is expected to change the response of the plate such that it must be considered in the dryer FEM.

5.2.2 Methods

The effect of cracking on the dynamic characteristics of the skirt adjacent to the drain channel weld DC-V3-320 and DC-V7-140 is assessed by performing parametric modal analyses of a plate with cracking assumed for various crack length to plate width ratios, a/W, and crack position to plate height ratios, x/H. Results for cases which bound the size and location of drain channel cracks observed in NMP2 will be used for the vibration assessment. Figure 5-19 illustrates the cracked plate configuration considered for this evaluation. Table 5-2 summarizes the range of a/W and x/H considered and introduces the format in which the modal frequencies from the cracked panel solutions will be presented.

The ANSYS finite element analysis program is used to perform this evaluation [14]. The 2-D elastic shell element, SHELL63, is used for this analysis. Cracking is simulated by meshing the geometry with coincident but uncoupled nodes along the crack face. Since the focus of this analysis is the change in stiffness and its effect on vibration modes of the skirt rather than the stress intensity factor at the tip of the assumed crack, no crack tip elements are incorporated into the model.

The frequency content of the acoustic loads acting upon the surfaces of the BWR steam dryers is typically less than ~250 Hz; therefore, it is considered sufficient to show that if the change in modal frequencies, for the modes below 250 Hz, are small then the effect on the dynamic characteristics of the component is small.

5.2.3 Results

Figure 5-20 shows the mesh and boundary conditions applied for a solution convergence check performed to ensure that the mesh density used was sufficient to resolve the modes of interest. Table 5-3 summarizes the modal frequencies for all modes less than 250 Hz and reports a percent change in predicted frequency for each mesh density. The results shown in Table 5-3 confirm that the baseline mesh density applied to the FEM is sufficient. All subsequent cracked panel analyses are performed using the mesh density and boundary conditions shown in Figure 5-20. The element size for this analysis is defined as 1 in. x 1 in. The refined mesh densities evaluated for the mesh check had element sizes of ½" x ½" and $^1/_3$" x $^1/_3$".

For illustrative purposes, Figure 5-21 shows the configuration of a crack considered in the panel for the a/W=0.3 and x/H=0.6 parametric case.

Tables 5-4 through 5-18 summarize the modal frequencies for all modes less than 250 Hz for all 20 parametric crack cases. Also shown in these tables are the ratios between the cracked frequency and the uncracked frequency for the same mode. Figures 5-4 through 5-18 graphically depict the frequency ratio over the parametric response surface. The results show that even for cracking extending ½ of the distance across the panel, the frequencies in the range of interest are reduced by less than 5%. The average reduction in natural frequency across all crack sizes and

locations considered and considering all modes less than 250 Hz is less than 1%. Considering the maximum crack length observed in the NMP2 drain channel weld, 1.6", the a/W for this case is 0.07. For a crack length to panel width ratio this small, the effect on the predicted natural frequencies of the cracked panel, in the frequency range for which significant modal participation is expected, is insignificant; therefore, no changes to the existing uncracked dryer FEM must be made to account for the drain channel cracking.

Figures 5-22 through 5-36 compare the cracked and uncracked mode shapes of the panel considered in this analysis for one of the 20 parametric cases evaluated (x/H=0.4, a/W=0.1). The results are illustrative of the effect of cracking on the dynamic characteristics of the panel for a flaw size which bounds the NMP2 drain channel indications. It is seen that cracking has an insignificant effect on the mode shape of the panel. Figure 5-37 shows the cracked mode shape for Mode 15 for the x/H=0.4 and a/W=0.3 parametric case. This plot illustrates that for higher modes and larger crack sizes, cracking will exhibit a greater effect on the mode shape local to the crack; however, even for this case, the overall mode shape remains substantially the same and the modal frequency exhibits only a very small change.

Table 5-1. Tabulation of Parametric Cracked Beam Calculations

a/W=0.075 — δ/L

	Baseline	0.00001	0.0001	0.001	0.002	0.004	0.008	0.01	0.02	0.04	0.1	0.2	0.4	0.5	0.6	0.7	0.8	0.9	1
C1_1_xx	-	0	0	0	0	0	0	0	0	0	0	0	0	0	0	0	0	0	0
C1_2_xx	-	0	0	0	0	0	0	0	0	0	0	0	0	0	0	0	0	0	0
C2_1_xx	-	-3.06E-08	-3.06E-07	-3.06E-06	-6.12E-06	-1.22E-05	-2.44E-05	-3.05E-05	-6.07E-05	-1.20E-04	-2.91E-04	-5.52E-04	-9.81E-04	-1.15E-03	-1.29E-03	-1.39E-03	-1.47E-03	-1.52E-03	-1.53E-03
C2_2_xx	-	1.53E-11	1.53E-09	1.53E-07	6.12E-07	2.45E-06	9.75E-06	1.52E-05	6.05E-05	2.39E-04	1.43E-03	5.31E-03	1.80E-02	2.55E-02	3.31E-02	4.00E-02	4.58E-02	4.96E-02	5.11E-02
Incremental Disp @ Cracked Section	-	0.000	0.000	0.000	0.000	0.000	0.000	0.000	0.000	-0.001	-0.007	-0.027	-0.101	-0.152	-0.211	-0.275	-0.343	-0.414	-0.487
Incremental Disp @ Uncracked Section	-0.385	-0.385	-0.385	-0.385	-0.386	-0.386	-0.388	-0.388	-0.391	-0.396	-0.406	-0.408	-0.364	-0.322	-0.270	-0.210	-0.143	-0.073	0.000
Max Displacement from Sum of Incremental		-0.385	-0.385	-0.385	-0.386	-0.386	-0.388	-0.388	-0.391	-0.397	-0.413	-0.435	-0.465	-0.475	-0.481	-0.485	-0.486	-0.487	-0.487
Max Displacment from Beam Solution		-0.385	-0.385	-0.385	-0.386	-0.386	-0.388	-0.388	-0.391	-0.397	-0.413	-0.435	-0.465	-0.475	-0.481	-0.485	-0.486	-0.487	-0.487
Displacement Ratio (cracked / uncracked)		1.000	1.000	1.001	1.002	1.003	1.006	1.008	1.016	1.031	1.072	1.129	1.208	1.232	1.248	1.258	1.263	1.265	1.265
Modulus Ratio (cracked / uncracked)		1.000	1.000	0.999	0.998	0.997	0.994	0.992	0.985	0.970	0.933	0.885	0.828	0.812	0.801	0.795	0.792	0.791	0.790

a/W=0.150 — δ/L

	Baseline	0.00001	0.0001	0.001	0.002	0.004	0.008	0.01	0.02	0.04	0.1	0.2	0.4	0.5	0.6	0.7	0.8	0.9	1
C1_1_xx	-	0	0	0	0	0	0	0	0	0	0	0	0	0	0	0	0	0	0
C1_2_xx	-	0	0	0	0	0	0	0	0	0	0	0	0	0	0	0	0	0	0
C2_1_xx	-	-7.26E-08	-7.26E-07	-7.26E-06	-1.45E-05	-2.90E-05	-5.78E-05	-7.22E-05	-1.44E-04	-2.85E-04	-6.90E-04	-1.31E-03	-2.32E-03	-2.72E-03	-3.05E-03	-3.30E-03	-3.48E-03	-3.59E-03	-3.63E-03
C2_2_xx	-	3.63E-11	3.63E-09	3.63E-07	1.45E-06	5.79E-06	2.31E-05	3.61E-05	1.43E-04	5.65E-04	3.39E-03	1.26E-02	4.26E-02	6.05E-02	7.84E-02	9.49E-02	1.08E-01	1.18E-01	1.21E-01
Incremental Disp @ Cracked Section	-	0.000	0.000	0.000	0.000	0.000	0.000	0.000	0.000	-0.001	-0.009	-0.035	-0.130	-0.196	-0.271	-0.353	-0.441	-0.533	-0.627
Incremental Disp @ Uncracked Section	-0.385	-0.385	-0.385	-0.386	-0.387	-0.388	-0.391	-0.392	-0.399	-0.412	-0.442	-0.468	-0.444	-0.401	-0.341	-0.267	-0.184	-0.094	0.000
Max Displacement from Sum of Incremental		-0.385	-0.385	-0.386	-0.387	-0.388	-0.391	-0.392	-0.399	-0.413	-0.451	-0.503	-0.575	-0.597	-0.612	-0.621	-0.625	-0.627	-0.627
Max Displacment from Beam Solution		-0.385	-0.385	-0.386	-0.387	-0.388	-0.391	-0.392	-0.399	-0.413	-0.451	-0.503	-0.575	-0.597	-0.612	-0.621	-0.625	-0.627	-0.627
Displacement Ratio (cracked / uncracked)		1.000	1.000	1.002	1.004	1.008	1.015	1.019	1.037	1.072	1.170	1.307	1.493	1.550	1.588	1.611	1.623	1.628	1.628
Modulus Ratio (cracked / uncracked)		1.000	1.000	0.998	0.996	0.993	0.985	0.982	0.964	0.932	0.854	0.765	0.670	0.645	0.630	0.621	0.616	0.614	0.614

a/W=0.300 — δ/L

	Baseline	0.00001	0.0001	0.001	0.002	0.004	0.008	0.01	0.02	0.04	0.1	0.2	0.4	0.5	0.6	0.7	0.8	0.9	1
C1_1_xx	-	0	0	0	0	0	0	0	0	0	0	0	0	0	0	0	0	0	0
C1_2_xx	-	0	0	0	0	0	0	0	0	0	0	0	0	0	0	0	0	0	0
C2_1_xx	-	-2.21E-07	-2.21E-06	-2.21E-05	-4.42E-05	-8.83E-05	-1.76E-04	-2.20E-04	-4.38E-04	-8.68E-04	-2.10E-03	-3.98E-03	-7.08E-03	-8.30E-03	-9.29E-03	-1.01E-02	-1.06E-02	-1.10E-02	-1.11E-02
C2_2_xx	-	1.11E-10	1.11E-08	1.11E-06	4.42E-06	1.77E-05	7.04E-05	1.10E-04	4.37E-04	1.72E-03	1.03E-02	3.84E-02	1.30E-01	1.84E-01	2.39E-01	2.89E-01	3.30E-01	3.59E-01	3.69E-01
Incremental Disp @ Cracked Section	-	0.000	0.000	0.000	0.000	0.000	0.000	0.000	-0.001	-0.003	-0.016	-0.063	-0.234	-0.351	-0.485	-0.633	-0.790	-0.955	-1.123
Incremental Disp @ Uncracked Section	-0.385	-0.385	-0.385	-0.387	-0.390	-0.394	-0.403	-0.407	-0.428	-0.467	-0.569	-0.682	-0.730	-0.680	-0.591	-0.470	-0.326	-0.167	0.000
Max Displacement from Sum of Incremental		-0.385	-0.385	-0.387	-0.390	-0.394	-0.403	-0.407	-0.428	-0.470	-0.585	-0.745	-0.963	-1.031	-1.076	-1.103	-1.117	-1.122	-1.123
Max Displacment from Beam Solution		-0.385	-0.385	-0.387	-0.390	-0.394	-0.403	-0.407	-0.428	-0.470	-0.585	-0.745	-0.963	-1.031	-1.076	-1.103	-1.117	-1.122	-1.123
Displacement Ratio (cracked / uncracked)		1.000	1.001	1.006	1.011	1.023	1.046	1.057	1.113	1.221	1.519	1.935	2.502	2.676	2.793	2.864	2.900	2.914	2.915
Modulus Ratio (cracked / uncracked)		1.000	0.999	0.994	0.989	0.978	0.956	0.946	0.899	0.819	0.658	0.517	0.400	0.374	0.358	0.349	0.345	0.343	0.343

a/W=0.600 — δ/L

	Baseline	0.00001	0.0001	0.001	0.002	0.004	0.008	0.01	0.02	0.04	0.1	0.2	0.4	0.5	0.6	0.7	0.8	0.9	1
C1_1_xx	-	0	0	0	0	0	0	0	0	0	0	0	0	0	0	0	0	0	0
C1_2_xx	-	0	0	0	0	0	0	0	0	0	0	0	0	0	0	0	0	0	0
C2_1_xx	-	-1.69E-06	-1.69E-05	-1.69E-04	-3.38E-04	-6.75E-04	-1.35E-03	-1.68E-03	-3.35E-03	-6.62E-03	-1.61E-02	-3.04E-02	-5.41E-02	-6.34E-02	-7.10E-02	-7.69E-02	-8.11E-02	-8.36E-02	-8.45E-02
C2_2_xx	-	8.45E-10	8.45E-08	8.44E-06	3.37E-05	1.35E-04	5.38E-04	8.39E-04	3.33E-03	1.32E-02	7.89E-02	2.93E-01	9.91E-01	1.41E+00	1.82E+00	2.21E+00	2.52E+00	2.74E+00	2.82E+00
Incremental Disp @ Cracked Section	-	0.000	0.000	0.000	0.000	0.000	-0.001	-0.001	-0.004	-0.014	-0.087	-0.337	-1.252	-1.880	-2.600	-3.391	-4.236	-5.118	-6.017
Incremental Disp @ Uncracked Section	-0.385	-0.385	-0.387	-0.402	-0.419	-0.452	-0.519	-0.552	-0.713	-1.020	-1.824	-2.797	-3.549	-3.433	-3.057	-2.475	-1.736	-0.894	0.000
Max Displacement from Sum of Incremental		-0.385	-0.387	-0.402	-0.419	-0.452	-0.519	-0.552	-0.716	-1.034	-1.911	-3.134	-4.801	-5.313	-5.657	-5.865	-5.972	-6.012	-6.017
Max Displacment from Beam Solution		-0.385	-0.387	-0.402	-0.419	-0.452	-0.519	-0.552	-0.716	-1.034	-1.911	-3.134	-4.801	-5.313	-5.657	-5.865	-5.972	-6.012	-6.017
Displacement Ratio (cracked / uncracked)		1.000	1.004	1.044	1.088	1.175	1.348	1.434	1.860	2.686	4.963	8.137	12.466	13.797	14.689	15.230	15.508	15.610	15.625
Modulus Ratio (cracked / uncracked)		1.000	0.996	0.958	0.919	0.851	0.742	0.697	0.538	0.372	0.201	0.123	0.080	0.072	0.068	0.066	0.064	0.064	0.064

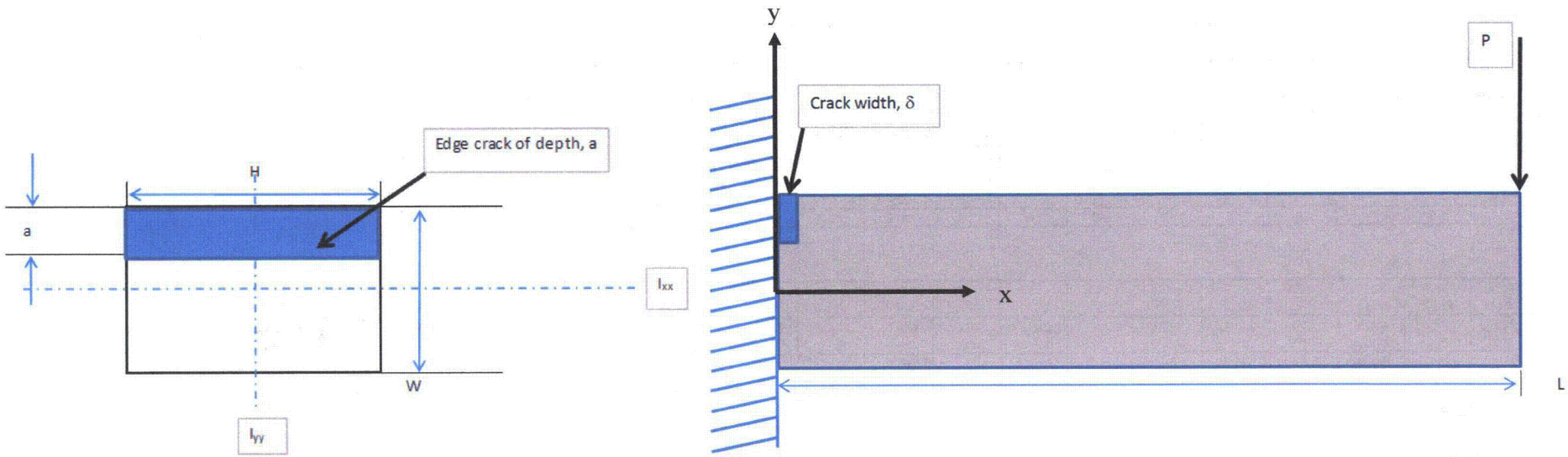

Note: For this analysis, bending is evaluated about the weak axis to maximize the effect of cracking; hence the orientation of the applied load and beam cross-section.

Figure 5-1. Composite Beam Composed of 1 Cracked and 1 Uncracked Section.

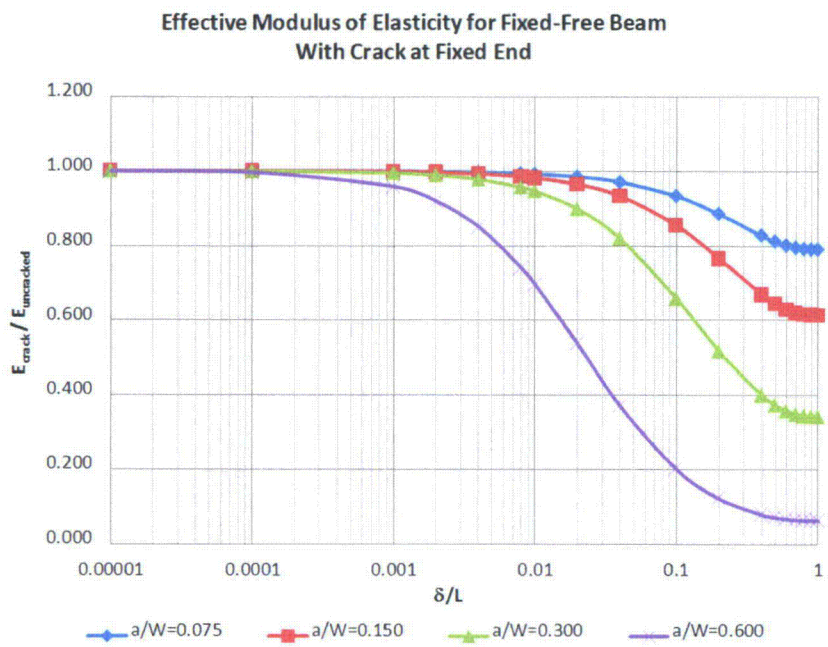

Figure 5-2. Ratio of Effective Elastic Modulus to Uncracked Elastic Modulus for a Cracked Beam for Various a/W and δ/L.

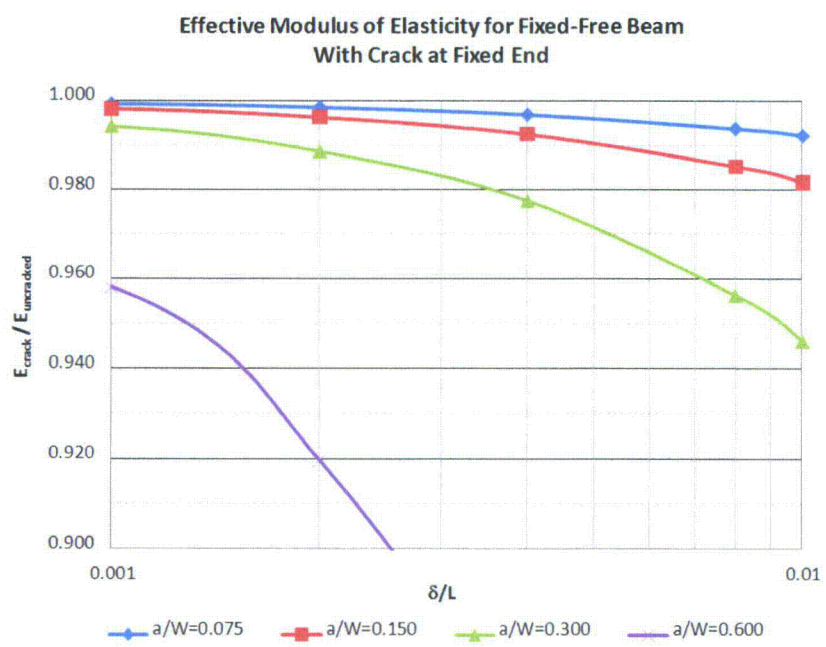

Figure 5-3. Ratio of Effective Elastic Modulus to Uncracked Elastic Modulus for a Cracked Beam for Various a/W and δ/L, Zoomed to NMP2 Effective δ/L.

Table 5-2. Matrix of Parametric Crack Cases Considered.

		a/W				
ω=i		0.1	0.2	0.3	0.4	0.5
x/H	0.2	Case 1	Case 2	Case 3	Case 4	Case 5
	0.4	Case 6	Case 7	Case 8	Case 9	Case 10
	0.6	Case 11	Case 12	Case 13	Case 14	Case 15
	0.8	Case 16	Case 17	Case 18	Case 19	Case 20

Note: 1. The baseline case for the uncracked structure is Case 21.

Table 5-3. Summary of Modal Frequencies < 250 Hz for Three Mesh Densities

	Mode 1	Mode 2	Mode 3	Mode 4	Mode 5	Mode 6	Mode 7	Mode 8
Mesh 1	42.23	47.83	58.72	74.73	95.81	122.01	153.36	167.40
Mesh 2	42.23	47.83	58.73	74.75	95.85	122.07	153.45	167.39
Mesh 3	42.24	47.88	58.85	74.99	96.25	122.66	154.28	167.39
% Change 1-2	0.00	0.00	0.02	0.03	0.04	0.05	0.06	-0.01
% Change 2-3	0.02	0.10	0.20	0.32	0.42	0.48	0.54	0.00

	Mode 9	Mode 10	Mode 11	Mode 12	Mode 13	Mode 14	Mode 15
Mesh 1	172.93	183.69	189.90	199.75	221.04	231.64	247.50
Mesh 2	172.95	183.74	190.03	199.84	221.19	231.82	247.73
Mesh 3	172.99	183.87	191.13	200.10	221.61	233.23	248.36
% Change 1-2	0.01	0.03	0.07	0.05	0.07	0.08	0.09
% Change 2-3	0.02	0.07	0.58	0.13	0.19	0.61	0.25

Table 5-4. Summary of Parametric Results for Mode 1 and Ratio of Cracked / Uncracked Frequencies

		a/W				
ω=1	**42.23 Hz**	**0.1**	**0.2**	**0.3**	**0.4**	**0.5**
x/H	**0.2**	42.23	42.23	42.22	42.18	42.12
	0.4	42.23	42.23	42.22	42.20	42.16
	0.6	42.23	42.23	42.23	42.22	42.20
	0.8	42.23	42.23	42.23	42.23	42.22

		a/W				
ω=1	**42.23 Hz**	**0.1**	**0.2**	**0.3**	**0.4**	**0.5**
x/H	**0.2**	1.000	1.000	1.000	0.999	0.997
	0.4	1.000	1.000	1.000	0.999	0.998
	0.6	1.000	1.000	1.000	1.000	0.999
	0.8	1.000	1.000	1.000	1.000	1.000

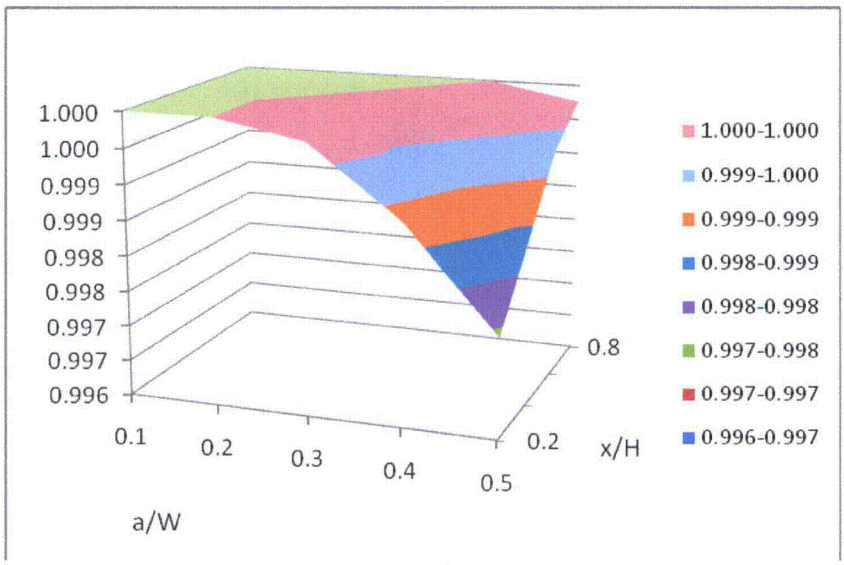

Figure 5-4. Ratio of Cracked / Uncracked Frequency, Mode 1.

Table 5-5. Summary of Parametric Results for Mode 2 and Ratio of Cracked / Uncracked Frequencies

		a/W				
ω=2	47.83 Hz	0.1	0.2	0.3	0.4	0.5
x/H	0.2	47.83	47.83	47.82	47.8	47.74
	0.4	47.83	47.83	47.82	47.78	47.71
	0.6	47.83	47.82	47.79	47.72	47.59
	0.8	47.83	47.83	47.81	47.77	47.69

		a/W				
ω=2	47.83 Hz	0.1	0.2	0.3	0.4	0.5
x/H	0.2	1.000	1.000	1.000	0.999	0.998
	0.4	1.000	1.000	1.000	0.999	0.997
	0.6	1.000	1.000	0.999	0.998	0.995
	0.8	1.000	1.000	1.000	0.999	0.997

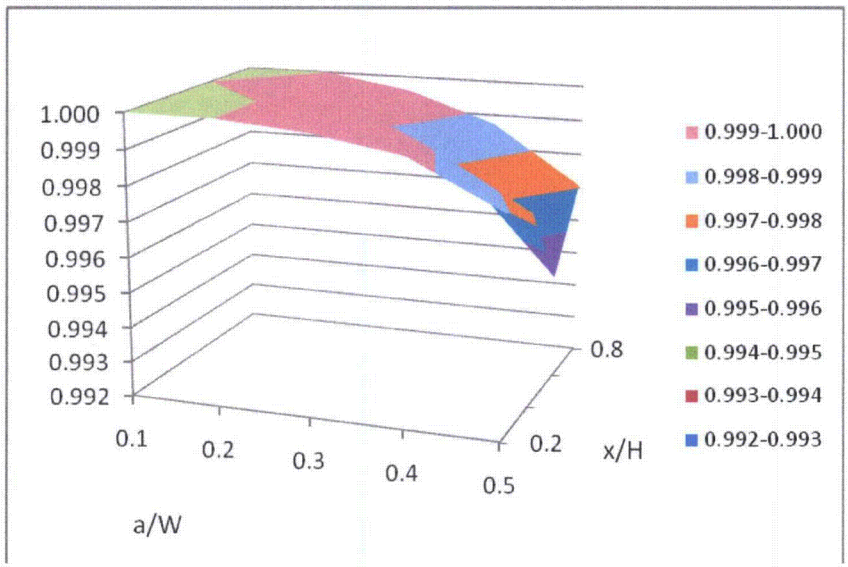

Figure 5-5. Ratio of Cracked / Uncracked Frequency, Mode 2.

Table 5-6. Summary of Parametric Results for Mode 3 and Ratio of Cracked / Uncracked Frequencies

		a/W				
ω=3	58.73 Hz	0.1	0.2	0.3	0.4	0.5
x/H	0.2	58.72	58.72	58.70	58.64	58.48
	0.4	58.72	58.70	58.65	58.51	58.27
	0.6	58.72	58.72	58.70	58.64	58.48
	0.8	58.72	58.71	58.66	58.53	58.29

		a/W				
ω=3	58.73 Hz	0.1	0.2	0.3	0.4	0.5
x/H	0.2	1.000	1.000	0.999	0.998	0.996
	0.4	1.000	0.999	0.999	0.996	0.992
	0.6	1.000	1.000	0.999	0.998	0.996
	0.8	1.000	1.000	0.999	0.997	0.993

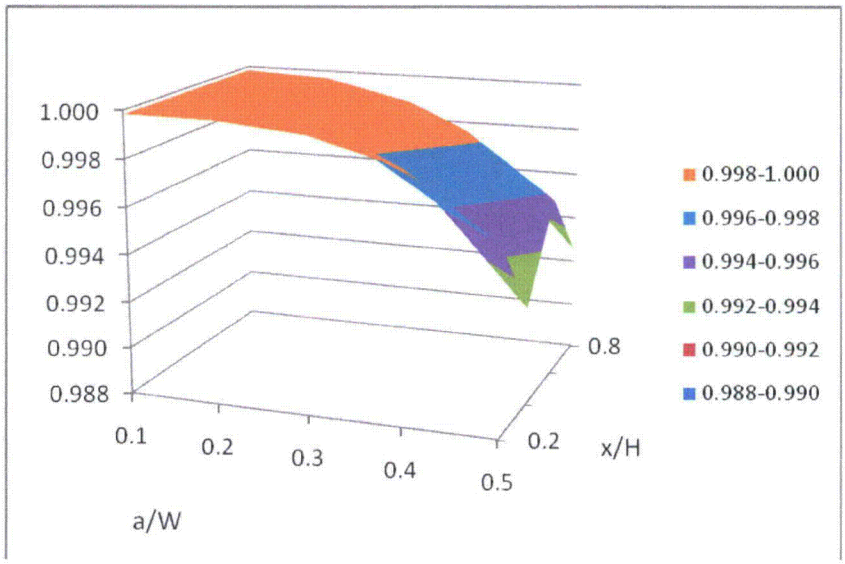

Figure 5-6. Ratio of Cracked / Uncracked Frequency, Mode 3.

Table 5-7. Summary of Parametric Results for Mode 4 and Ratio of Cracked / Uncracked Frequencies

		a/W				
ω=4	74.75 Hz	0.1	0.2	0.3	0.4	0.5
x/H	0.2	74.73	74.71	74.62	74.39	73.94
	0.4	74.73	74.73	74.71	74.61	74.28
	0.6	74.73	74.71	74.65	74.45	74.05
	0.8	74.73	74.70	74.60	74.35	73.90

		a/W				
ω=4	74.75 Hz	0.1	0.2	0.3	0.4	0.5
x/H	0.2	1.000	0.999	0.998	0.995	0.989
	0.4	1.000	1.000	0.999	0.998	0.994
	0.6	1.000	0.999	0.999	0.996	0.991
	0.8	1.000	0.999	0.998	0.995	0.989

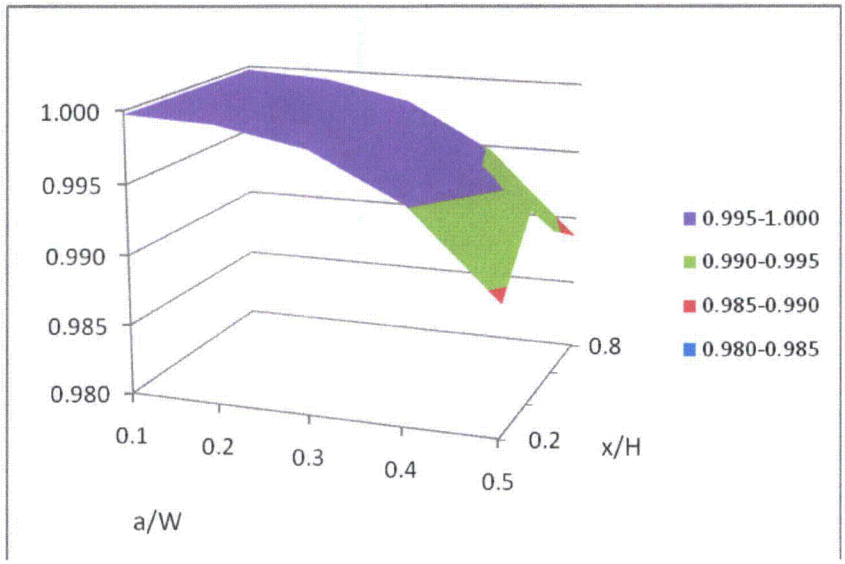

Figure 5-7. Ratio of Cracked / Uncracked Frequency, Mode 4.

Table 5-8. Summary of Parametric Results for Mode 5 and Ratio of Cracked / Uncracked Frequencies

		a/W				
ω=5	**95.85 Hz**	**0.1**	**0.2**	**0.3**	**0.4**	**0.5**
x/H	**0.2**	95.81	95.77	95.59	95.14	94.35
	0.4	95.81	95.77	95.60	95.15	94.37
	0.6	95.81	95.78	95.63	95.22	94.48
	0.8	95.81	95.79	95.68	95.36	94.68

		a/W				
ω=5	**95.85 Hz**	**0.1**	**0.2**	**0.3**	**0.4**	**0.5**
x/H	**0.2**	1.000	0.999	0.997	0.993	0.984
	0.4	1.000	0.999	0.997	0.993	0.985
	0.6	1.000	0.999	0.998	0.993	0.986
	0.8	1.000	0.999	0.998	0.995	0.988

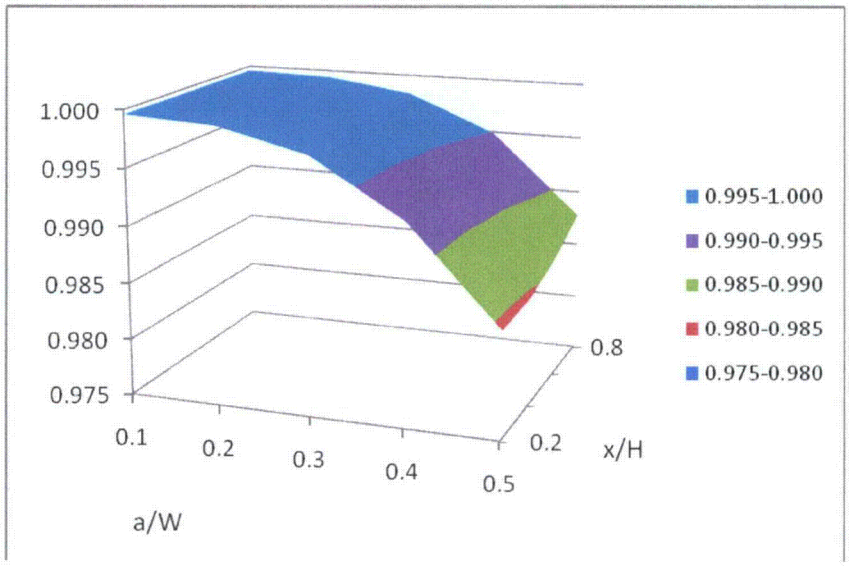

Figure 5-8. Ratio of Cracked / Uncracked Frequency, Mode 5.

Table 5-9. Summary of Parametric Results for Mode 6 and Ratio of Cracked / Uncracked Frequencies

		a/W				
ω=6	122.01 Hz	0.1	0.2	0.3	0.4	0.5
x/H	0.2	122.00	121.98	121.82	121.32	120.16
	0.4	122.01	122.00	121.90	121.51	120.35
	0.6	122.01	122.00	121.94	121.61	120.44
	0.8	122.01	122.00	121.93	121.57	120.44

		a/W				
ω=6	122.01 Hz	0.1	0.2	0.3	0.4	0.5
x/H	0.2	1.000	1.000	0.998	0.994	0.985
	0.4	1.000	1.000	0.999	0.996	0.986
	0.6	1.000	1.000	0.999	0.997	0.987
	0.8	1.000	1.000	0.999	0.996	0.987

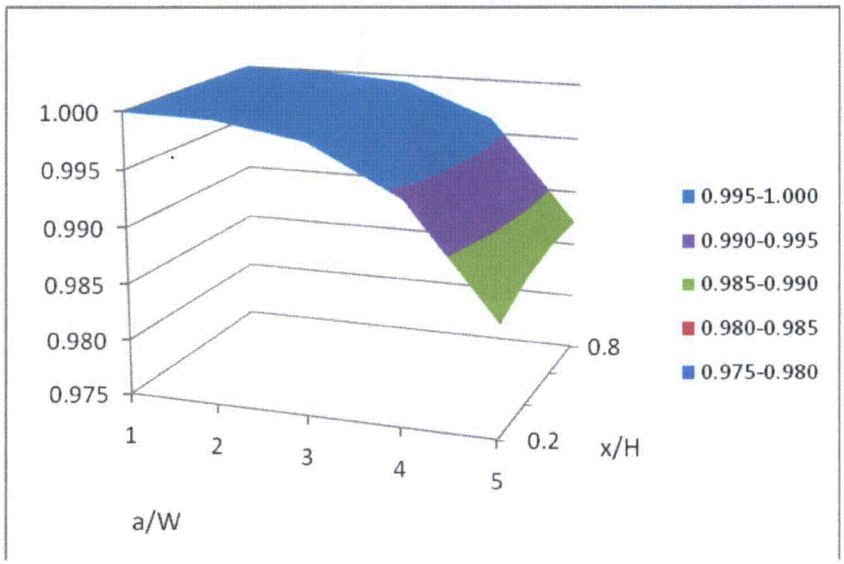

Figure 5-9. Ratio of Cracked / Uncracked Frequency, Mode 6.

Table 5-10. Summary of Parametric Results for Mode 7 and Ratio of Cracked / Uncracked Frequencies

		a/W				
ω=7	153.36 Hz	0.1	0.2	0.3	0.4	0.5
x/H	0.2	153.35	153.35	153.25	152.66	150.38
	0.4	153.35	153.30	153.02	152.15	150.21
	0.6	153.35	153.27	152.90	151.89	150.12
	0.8	153.35	153.34	153.21	152.58	150.39

		a/W				
ω=7	153.36 Hz	0.1	0.2	0.3	0.4	0.5
x/H	0.2	1.000	1.000	0.999	0.995	0.981
	0.4	1.000	1.000	0.998	0.992	0.979
	0.6	1.000	0.999	0.997	0.990	0.979
	0.8	1.000	1.000	0.999	0.995	0.981

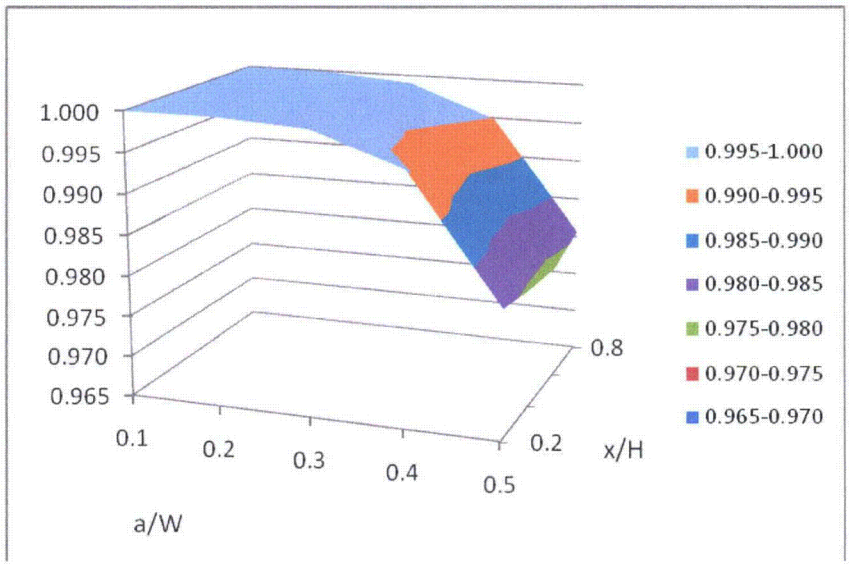

Figure 5-10. Ratio of Cracked / Uncracked Frequency, Mode 7.

Table 5-11. Summary of Parametric Results for Mode 8 and Ratio of Cracked / Uncracked Frequencies

		a/W				
ω=8	167.40 Hz	0.1	0.2	0.3	0.4	0.5
x/H	0.2	167.39	167.35	167.21	166.98	166.80
	0.4	167.39	167.37	167.29	167.16	167.00
	0.6	167.39	167.38	167.35	167.29	167.24
	0.8	167.39	167.39	167.38	167.36	167.31

		a/W				
ω=8	167.40 Hz	0.1	0.2	0.3	0.4	0.5
x/H	0.2	1.000	1.000	0.999	0.997	0.996
	0.4	1.000	1.000	0.999	0.999	0.998
	0.6	1.000	1.000	1.000	0.999	0.999
	0.8	1.000	1.000	1.000	1.000	0.999

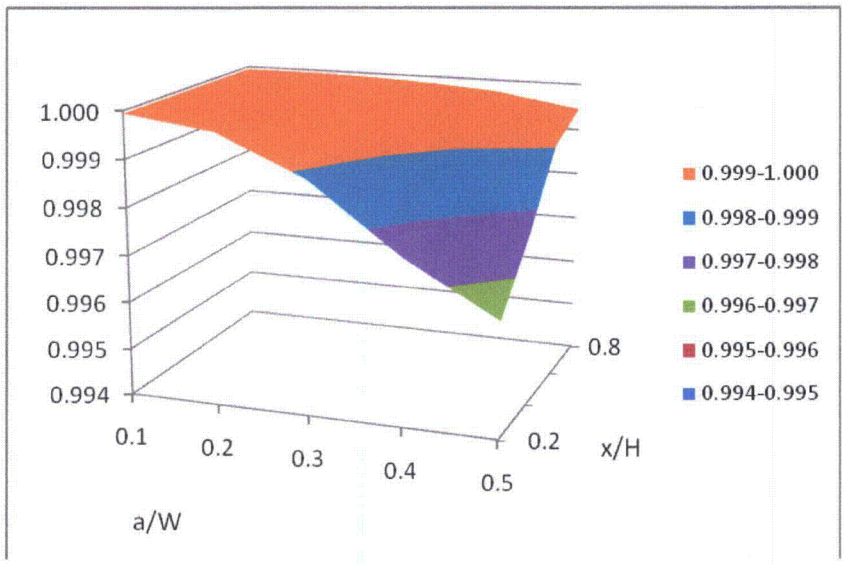

Figure 5-11. Ratio of Cracked / Uncracked Frequency, Mode 8.

Table 5-12. Summary of Parametric Results for Mode 9 and Ratio of Cracked / Uncracked Frequencies

		a/W				
ω=9	172.93 Hz	0.1	0.2	0.3	0.4	0.5
x/H	0.2	172.92	172.91	172.85	172.70	172.30
	0.4	172.92	172.91	172.83	172.66	172.30
	0.6	172.92	172.86	172.69	172.42	172.18
	0.8	172.92	172.89	172.77	172.52	172.11

		a/W				
ω=9	172.93 Hz	0.1	0.2	0.3	0.4	0.5
x/H	0.2	1.000	1.000	1.000	0.999	0.996
	0.4	1.000	1.000	0.999	0.998	0.996
	0.6	1.000	1.000	0.999	0.997	0.996
	0.8	1.000	1.000	0.999	0.998	0.995

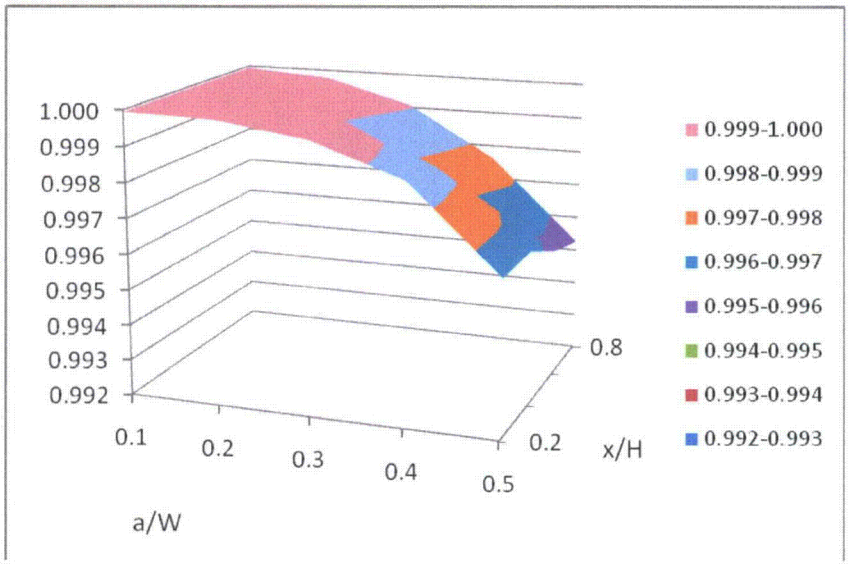

Figure 5-12. Ratio of Cracked / Uncracked Frequency, Mode 9.

Table 5-13. Summary of Parametric Results for Mode 10 and Ratio of Cracked / Uncracked Frequencies

		a/W				
ω=10	183.69 Hz	0.1	0.2	0.3	0.4	0.5
x/H	0.2	183.69	183.68	183.56	183.01	180.6
	0.4	183.69	183.62	183.37	182.86	181.68
	0.6	183.69	183.68	183.56	183.01	180.22
	0.8	183.69	183.62	183.36	182.83	181.91

		a/W				
ω=10	183.69 Hz	0.1	0.2	0.3	0.4	0.5
x/H	0.2	1.000	1.000	0.999	0.996	0.983
	0.4	1.000	1.000	0.998	0.995	0.989
	0.6	1.000	1.000	0.999	0.996	0.981
	0.8	1.000	1.000	0.998	0.995	0.990

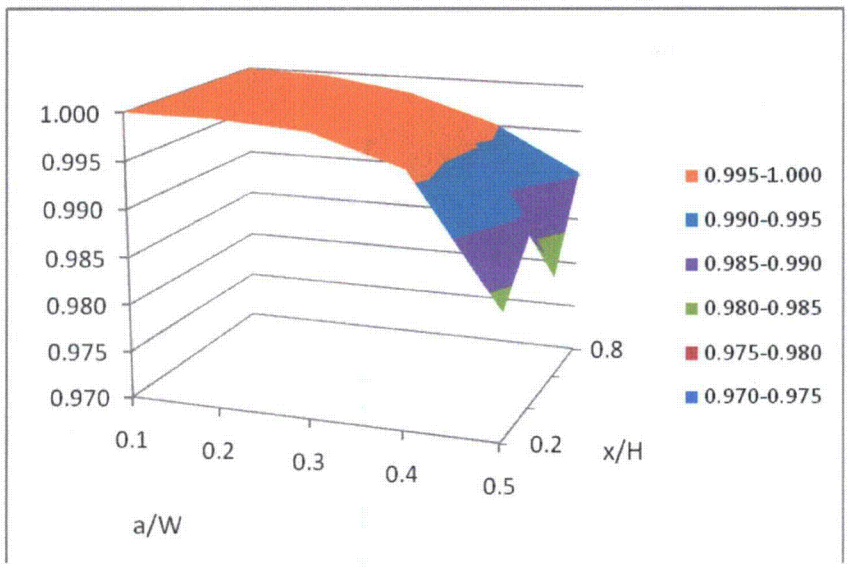

Figure 5-13. Ratio of Cracked / Uncracked Frequency, Mode 10.

Table 5-14. Summary of Parametric Results for Mode 11 and Ratio of Cracked / Uncracked Frequencies

		a/W				
ω=11	189.90 Hz	0.1	0.2	0.3	0.4	0.5
x/H	0.2	189.89	189.85	189.56	188.45	186.25
	0.4	189.89	189.81	189.43	188.33	185.88
	0.6	189.89	189.85	189.56	188.55	186.49
	0.8	189.88	189.81	189.43	188.36	186.36

		a/W				
ω=11	189.90 Hz	0.1	0.2	0.3	0.4	0.5
x/H	0.2	1.000	1.000	0.998	0.992	0.981
	0.4	1.000	1.000	0.998	0.992	0.979
	0.6	1.000	1.000	0.998	0.993	0.982
	0.8	1.000	1.000	0.998	0.992	0.981

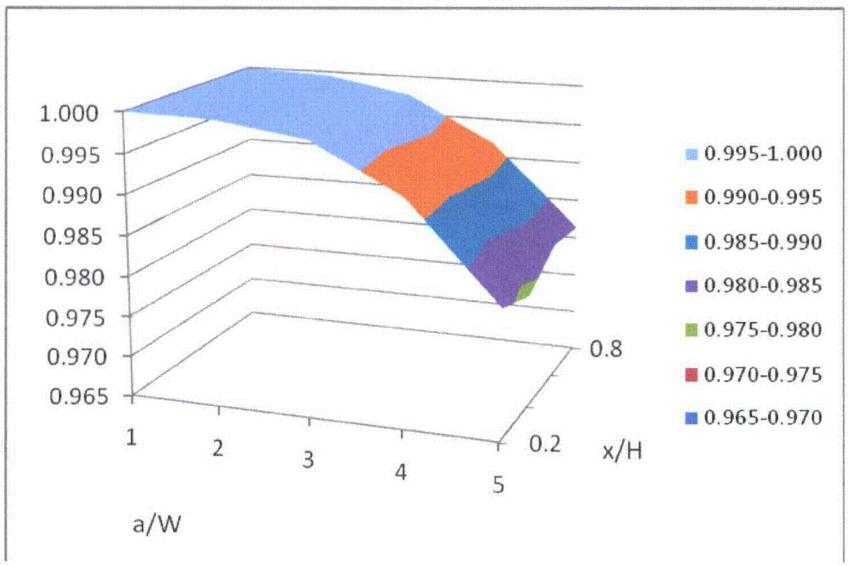

Figure 5-14. Ratio of Cracked / Uncracked Frequency, Mode 11.

Table 5-15. Summary of Parametric Results for Mode 12 and Ratio of Cracked / Uncracked Frequencies

		a/W				
ω=12	199.75 Hz	0.1	0.2	0.3	0.4	0.5
x/H	0.2	199.75	199.68	199.40	198.83	198.24
	0.4	199.75	199.73	199.52	198.61	196.02
	0.6	199.75	199.68	199.38	198.73	197.55
	0.8	199.75	199.66	199.35	198.77	197.68

		a/W				
ω=12	199.75 Hz	0.1	0.2	0.3	0.4	0.5
x/H	0.2	1.000	1.000	0.998	0.995	0.992
	0.4	1.000	1.000	0.999	0.994	0.981
	0.6	1.000	1.000	0.998	0.995	0.989
	0.8	1.000	1.000	0.998	0.995	0.990

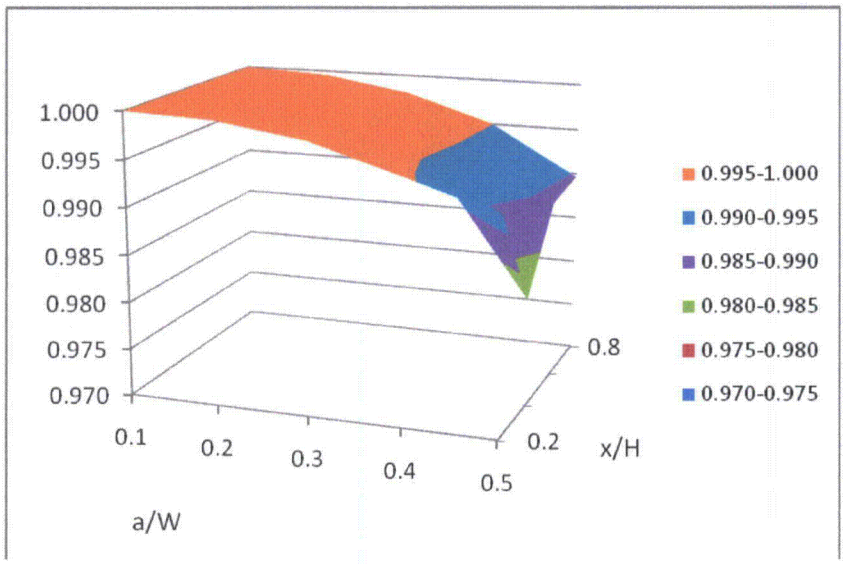

Figure 5-15. Ratio of Cracked / Uncracked Frequency, Mode 12.

Table 5-16. Summary of Parametric Results for Mode 13 and Ratio of Cracked / Uncracked Frequencies

		a/W				
ω=13	221.04 Hz	0.1	0.2	0.3	0.4	0.5
x/H	0.2	221.03	220.89	220.37	219.41	218.28
	0.4	221.04	220.91	220.44	219.53	217.09
	0.6	221.04	220.94	220.50	219.49	216.49
	0.8	221.04	220.97	220.55	219.06	214.31

		a/W				
ω=13	221.04 Hz	0.1	0.2	0.3	0.4	0.5
x/H	0.2	1.000	0.999	0.997	0.993	0.988
	0.4	1.000	0.999	0.997	0.993	0.982
	0.6	1.000	1.000	0.998	0.993	0.979
	0.8	1.000	1.000	0.998	0.991	0.970

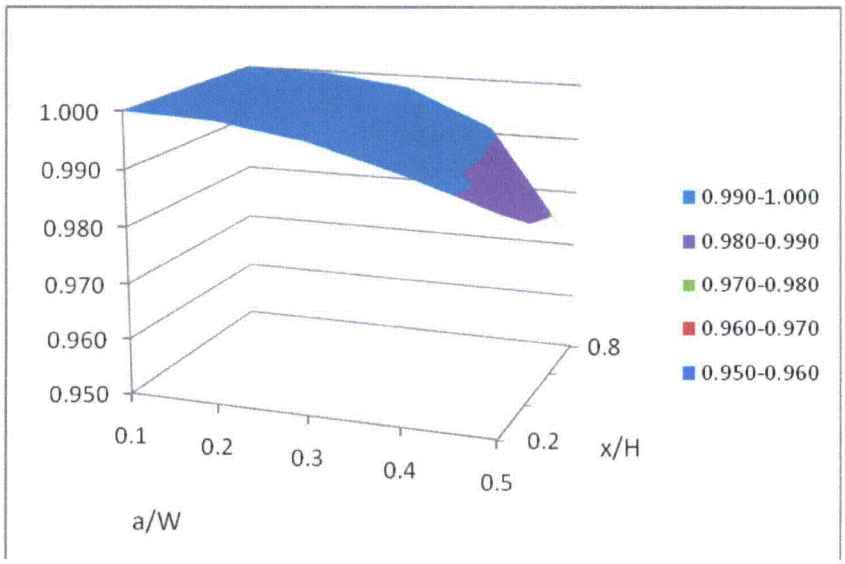

Figure 5-16. Ratio of Cracked / Uncracked Frequency, Mode 13.

Table 5-17. Summary of Parametric Results for Mode 14 and Ratio of Cracked / Uncracked Frequencies

		a/W				
ω=14	231.64 Hz	0.1	0.2	0.3	0.4	0.5
x/H	0.2	231.62	231.49	230.88	229.42	227.28
	0.4	231.63	231.61	231.32	229.73	224.13
	0.6	231.63	231.58	231.19	229.32	223.55
	0.8	231.62	231.48	230.81	229.20	226.66

		a/W				
ω=14	231.64 Hz	0.1	0.2	0.3	0.4	0.5
x/H	0.2	1.000	0.999	0.997	0.990	0.981
	0.4	1.000	1.000	0.999	0.992	0.968
	0.6	1.000	1.000	0.998	0.990	0.965
	0.8	1.000	0.999	0.996	0.989	0.979

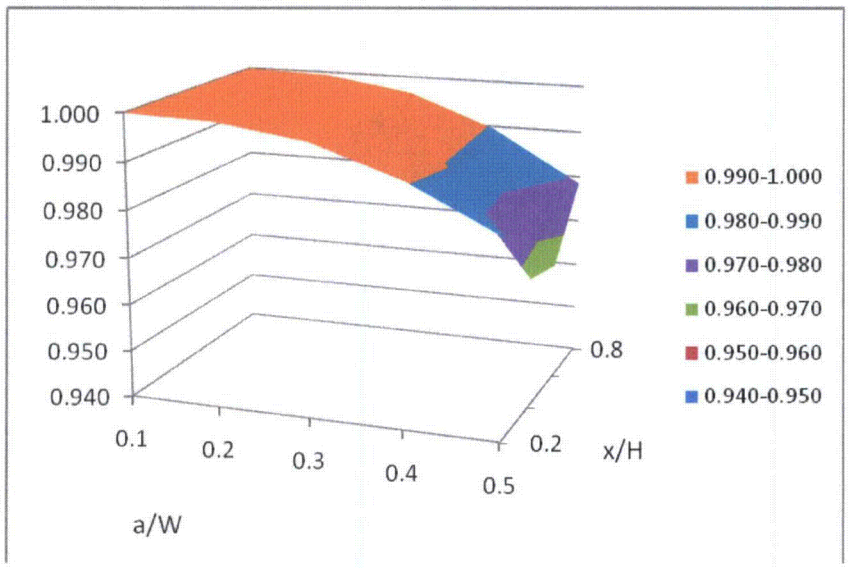

Figure 5-17. Ratio of Cracked / Uncracked Frequency, Mode 14.

Table 5-18. Summary of Parametric Results for Mode 15 and Ratio of Cracked / Uncracked Frequencies

		a/W				
ω=15	247.50 Hz	0.1	0.2	0.3	0.4	0.5
x/H	0.2	247.50	247.35	246.72	244.92	238.02
	0.4	247.50	247.41	246.79	244.75	241.17
	0.6	247.51	247.45	246.87	244.67	240.94
	0.8	247.51	247.46	246.87	244.10	236.20

		a/W				
ω=15	247.50 Hz	0.1	0.2	0.3	0.4	0.5
x/H	0.2	1.000	0.999	0.997	0.990	0.962
	0.4	1.000	1.000	0.997	0.989	0.974
	0.6	1.000	1.000	0.997	0.989	0.973
	0.8	1.000	1.000	0.997	0.986	0.954

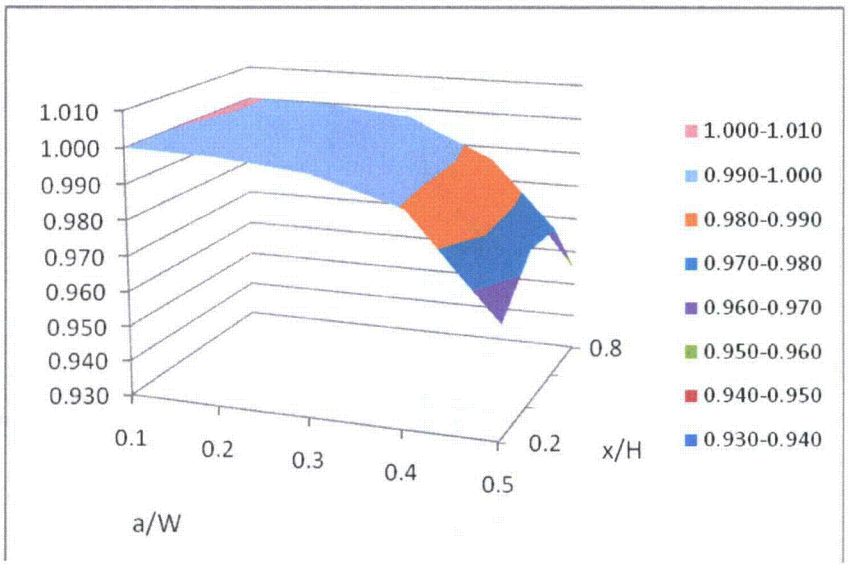

Figure 5-18. Ratio of Cracked / Uncracked Frequency, Mode 15.

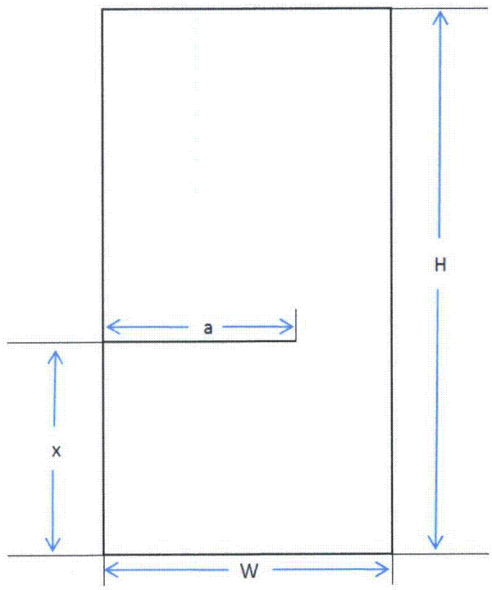

Figure 5-19. Crack Configuration Evaluated for NMP2 Drain Channel Cracking..

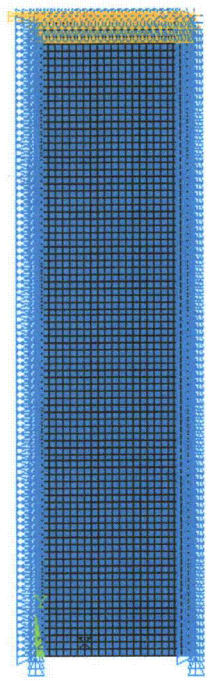

Figure 5-20. Mesh Density and Boundary Conditions Selected for Modal Analysis of Cracked Panel

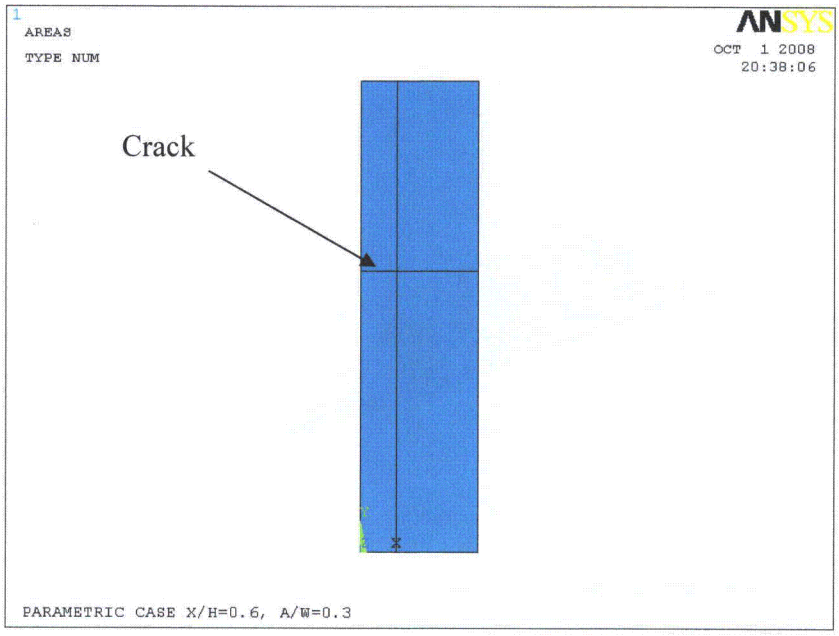

Figure 5-21. Sample Panel Area Showing Location of Crack in Panel.

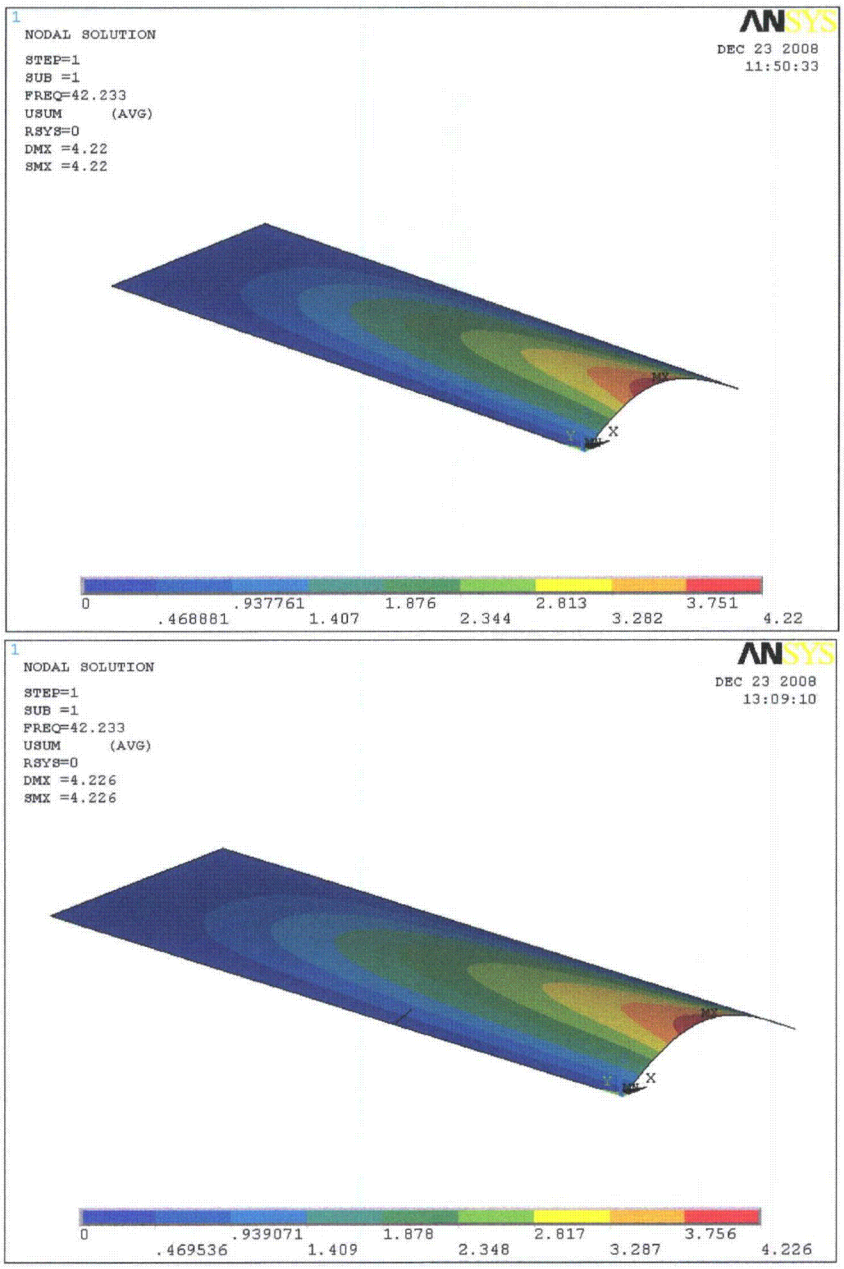

Figure 5-22. Modal Comparison Between Uncracked (Top) and Cracked (Bottom) Panels, Mode 1, x/H=0.4, a/W=0.1.

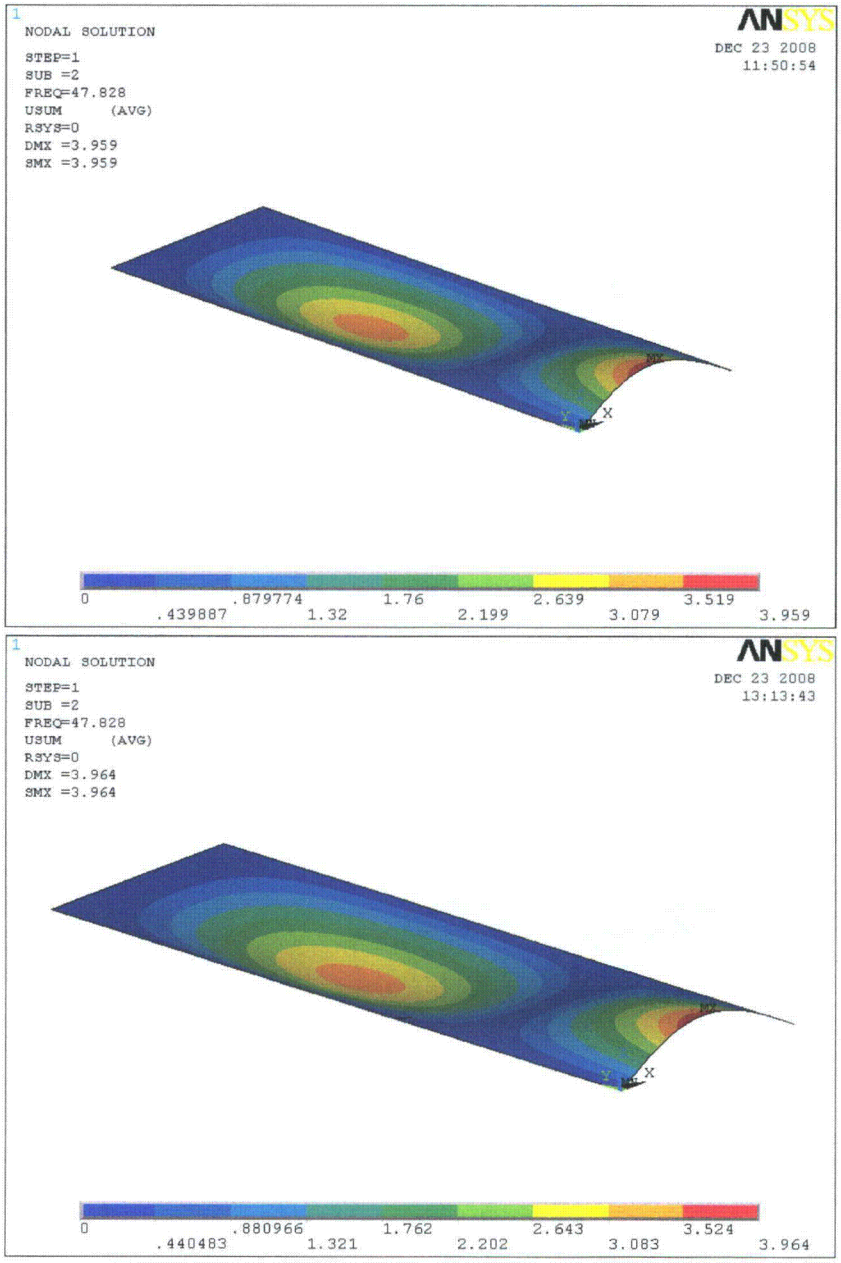

Figure 5-23. Modal Comparison Between Uncracked (Top) and Cracked (Bottom) Panels, Mode 2, x/H=0.4, a/W=0.1.

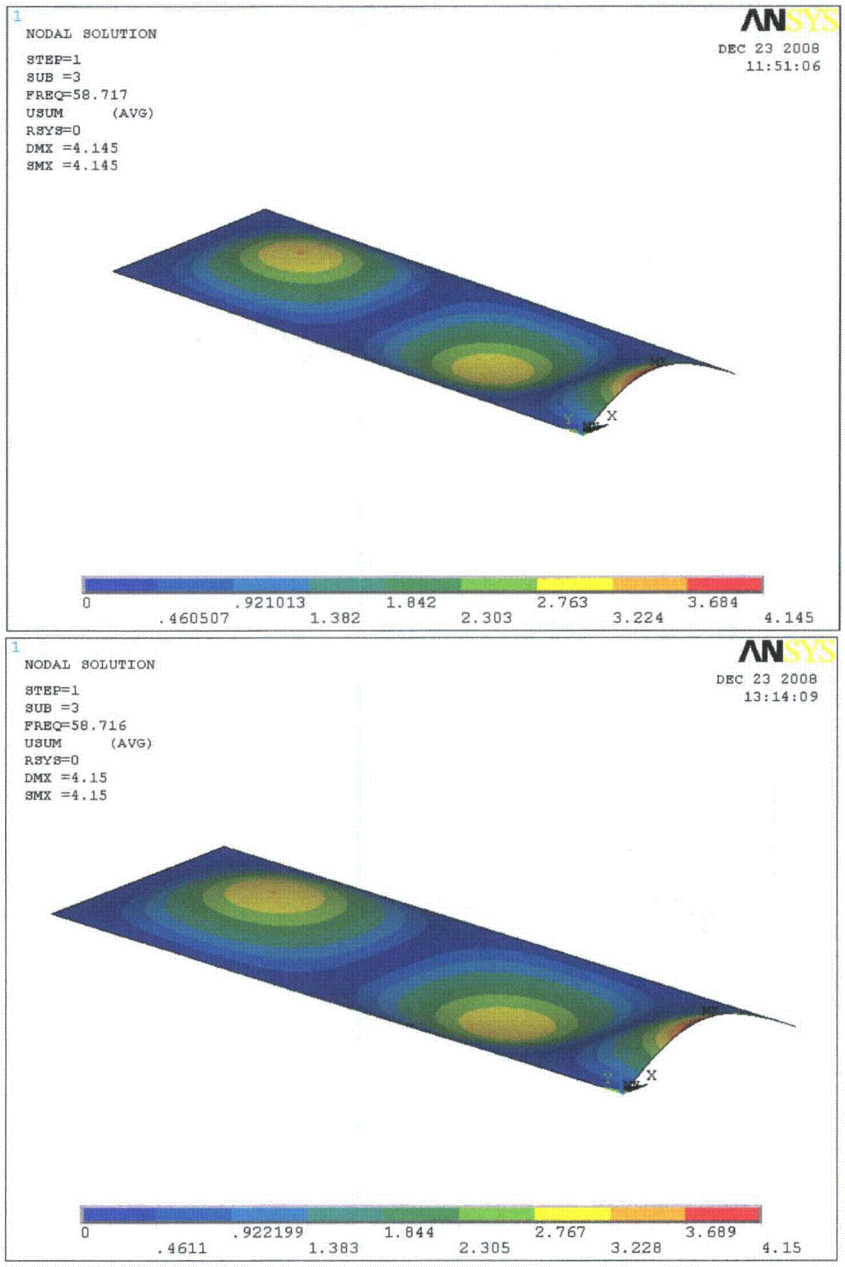

Figure 5-24. Modal Comparison Between Uncracked (Top) and Cracked (Bottom) Panels, Mode 3, x/H=0.4, a/W=0.1.

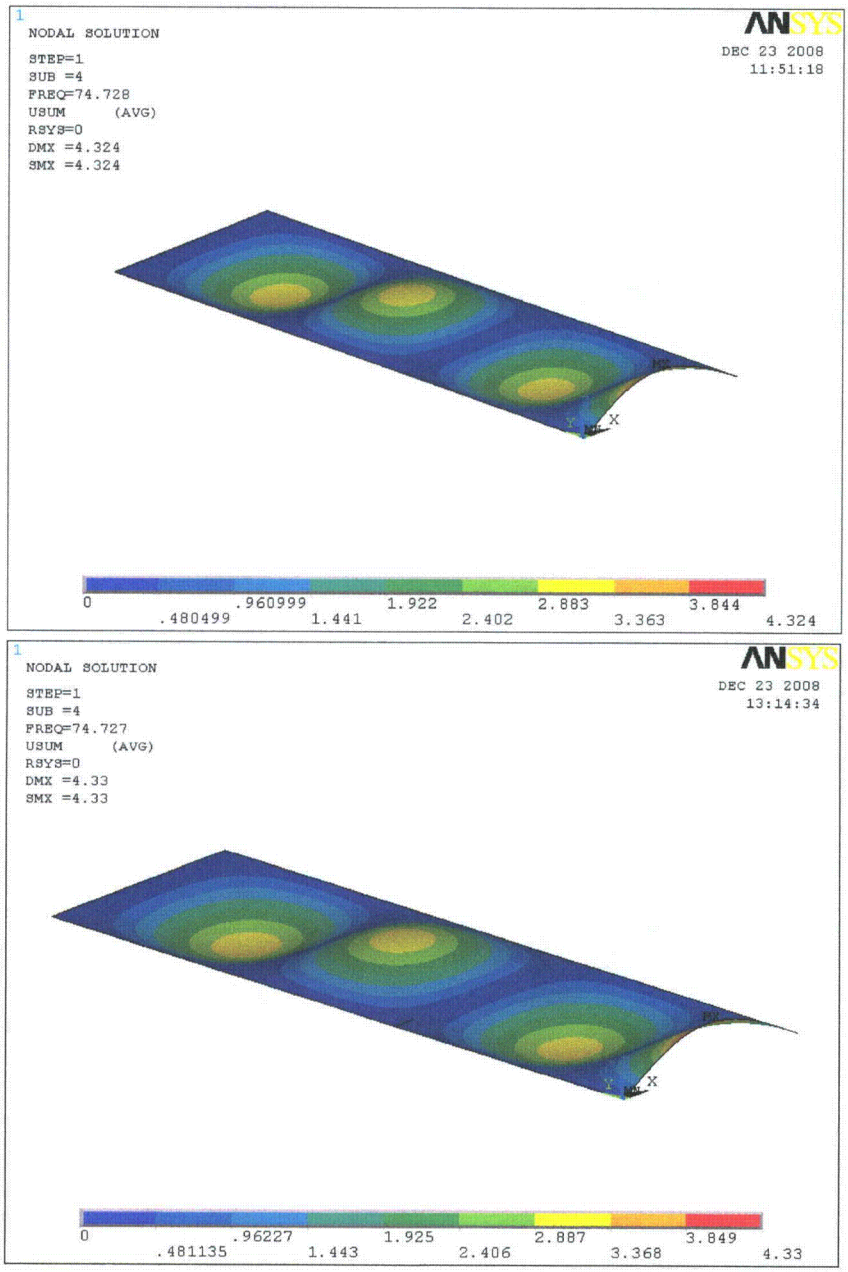

Figure 5-25. Modal Comparison Between Uncracked (Top) and Cracked (Bottom) Panels, Mode 4, x/H=0.4, a/W=0.1.

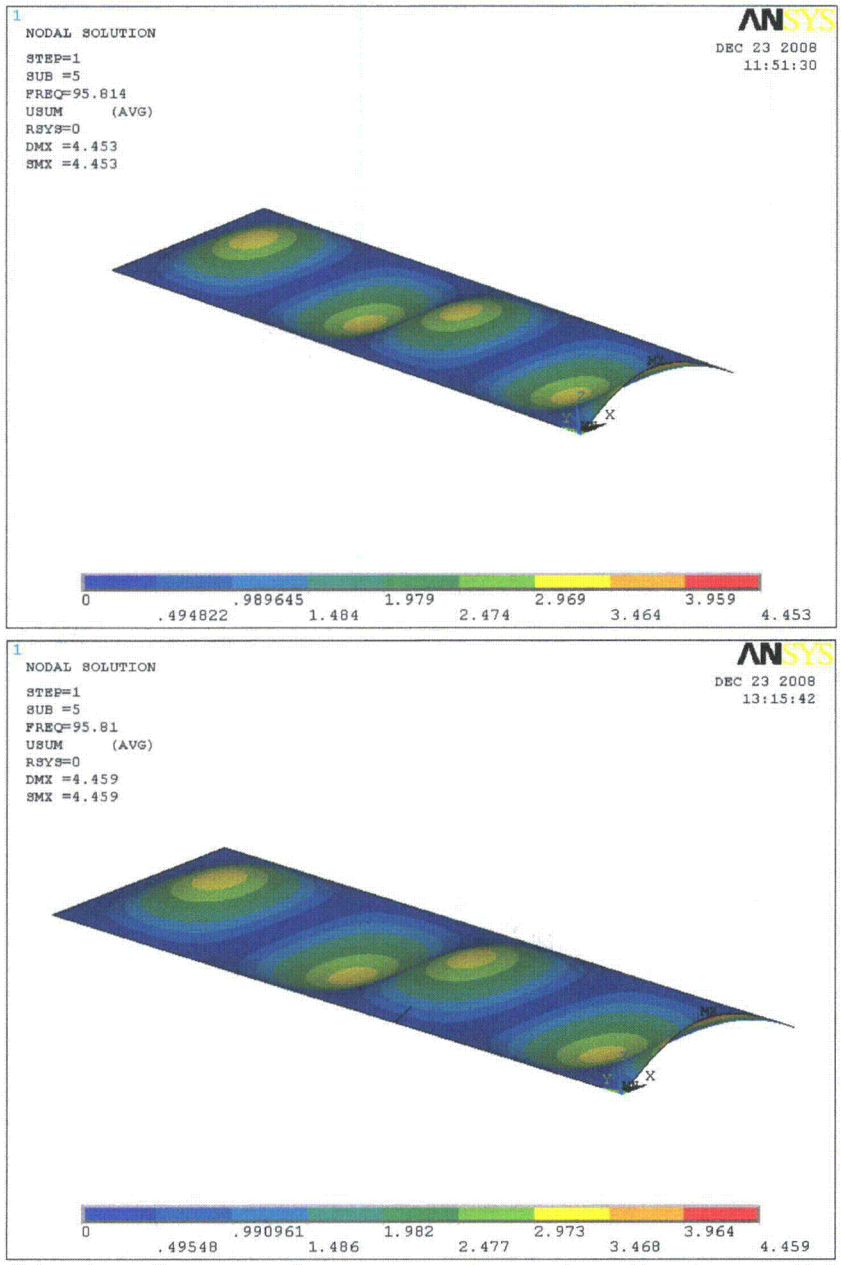

Figure 5-26. Modal Comparison Between Uncracked (Top) and Cracked (Bottom) Panels, Mode 5, x/H=0.4, a/W=0.1.

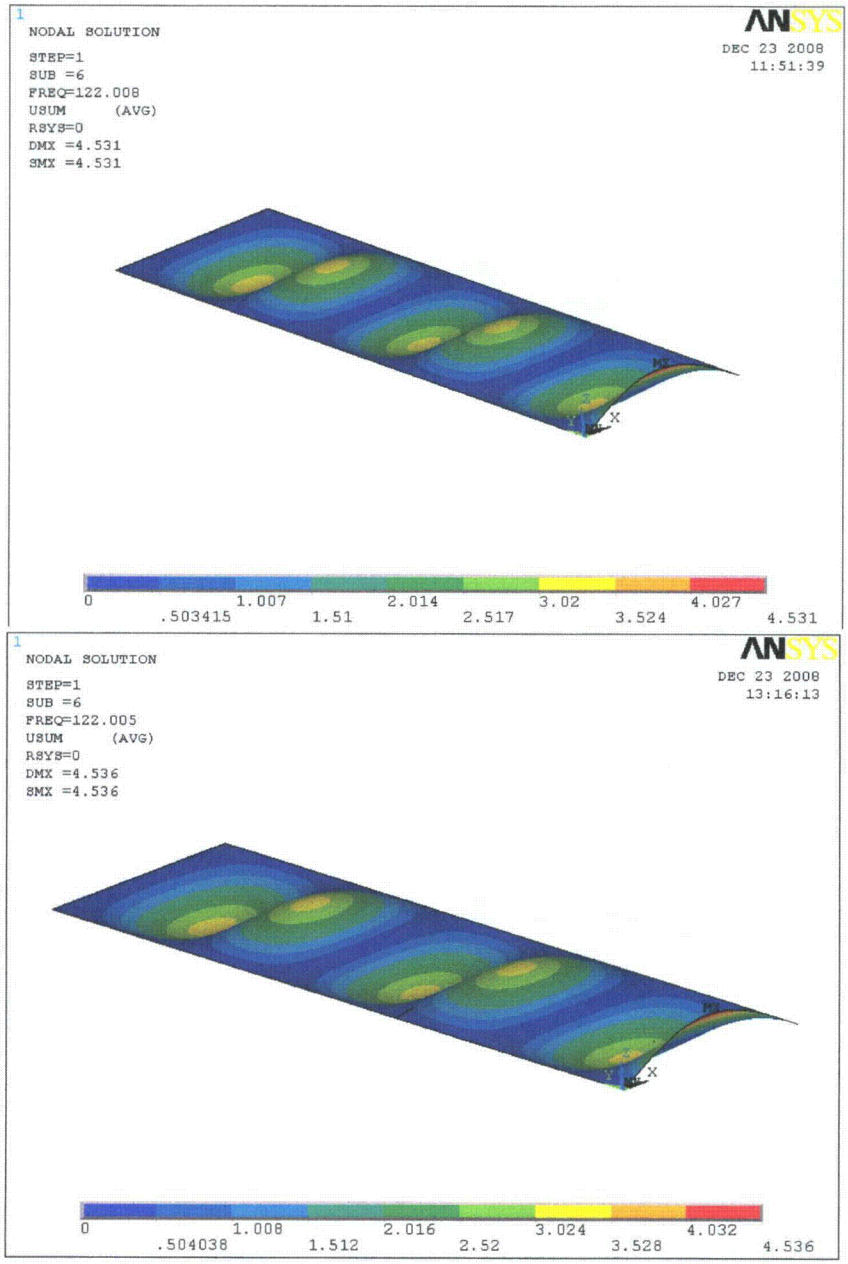

Figure 5-27. Modal Comparison Between Uncracked (Top) and Cracked (Bottom) Panels, Mode 6, x/H=0.4, a/W=0.1.

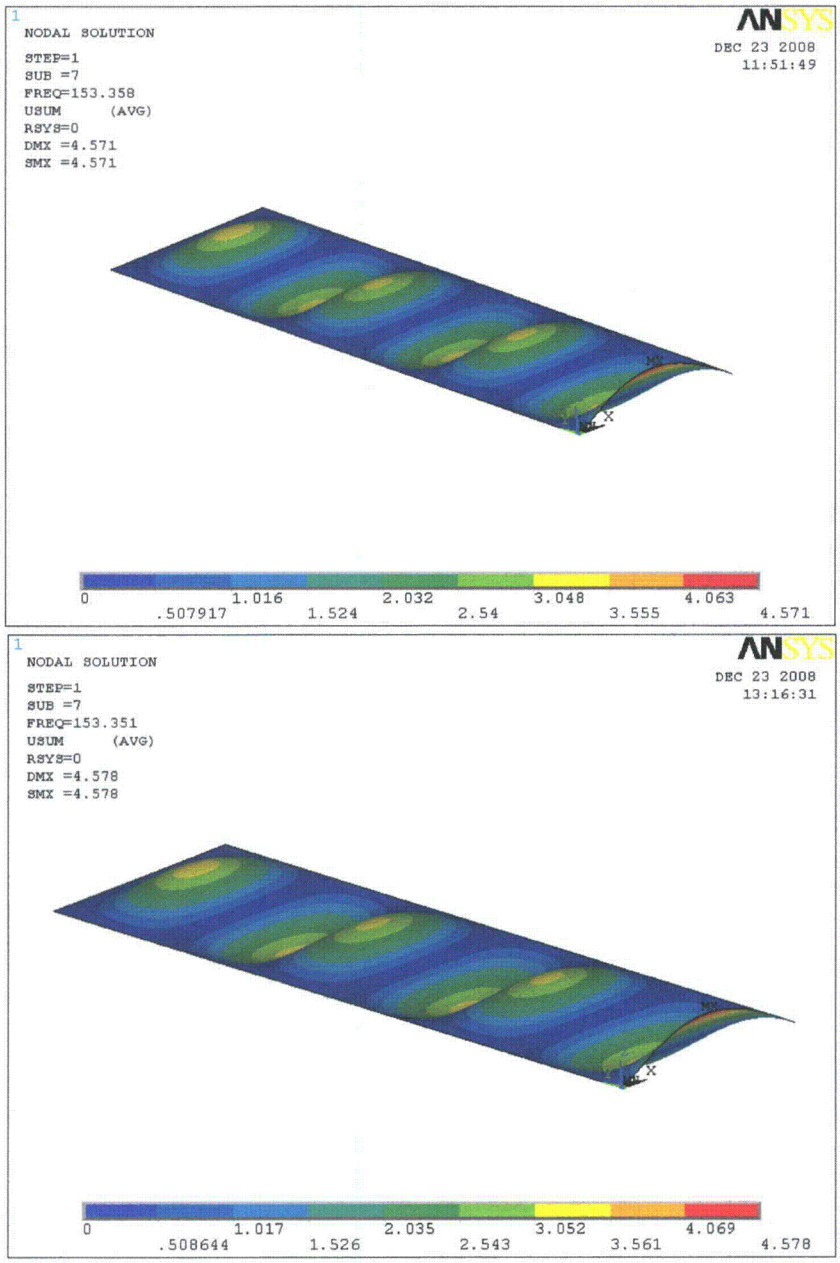

Figure 5-28. Modal Comparison Between Uncracked (Top) and Cracked (Bottom) Panels, Mode 7, x/H=0.4, a/W=0.1.

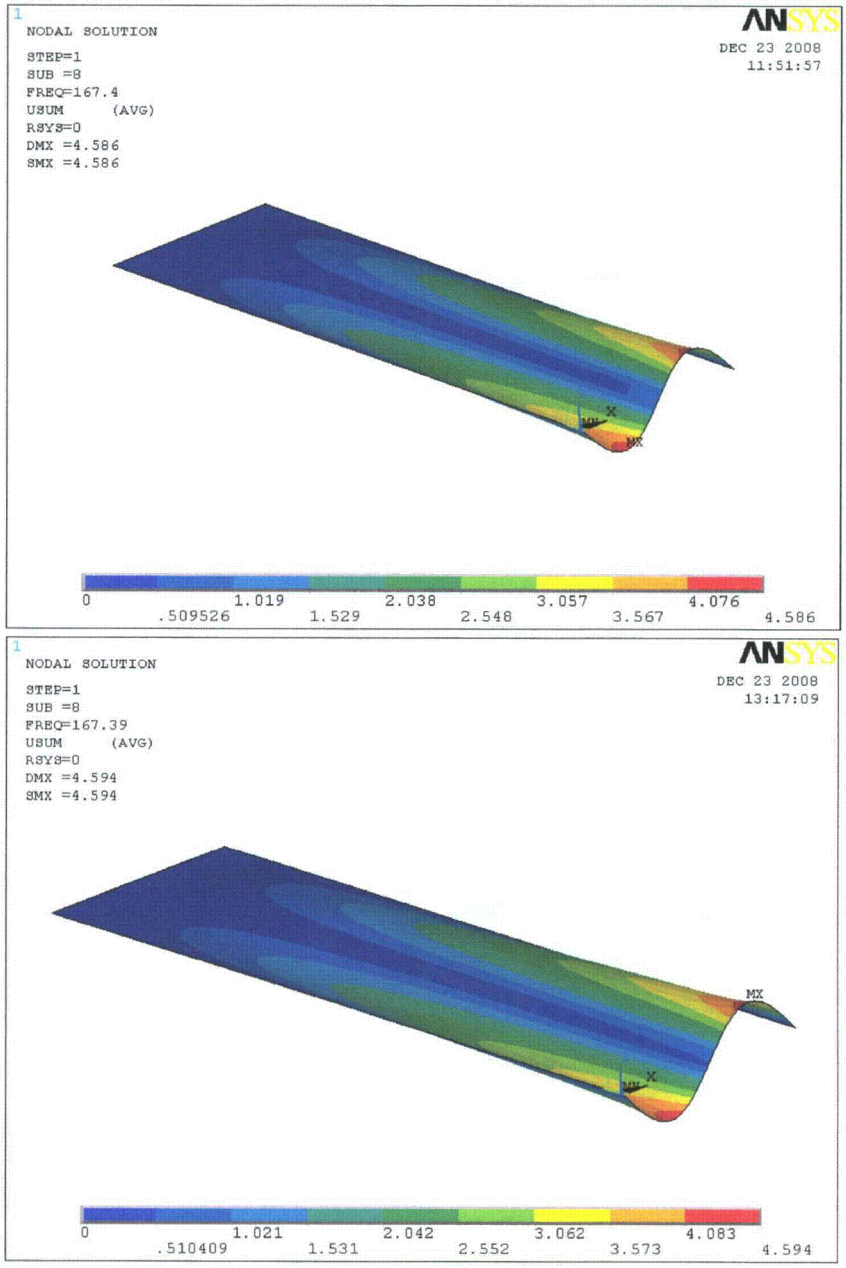

Figure 5-29. Modal Comparison Between Uncracked (Top) and Cracked (Bottom) Panels, Mode 8, x/H=0.4, a/W=0.1.

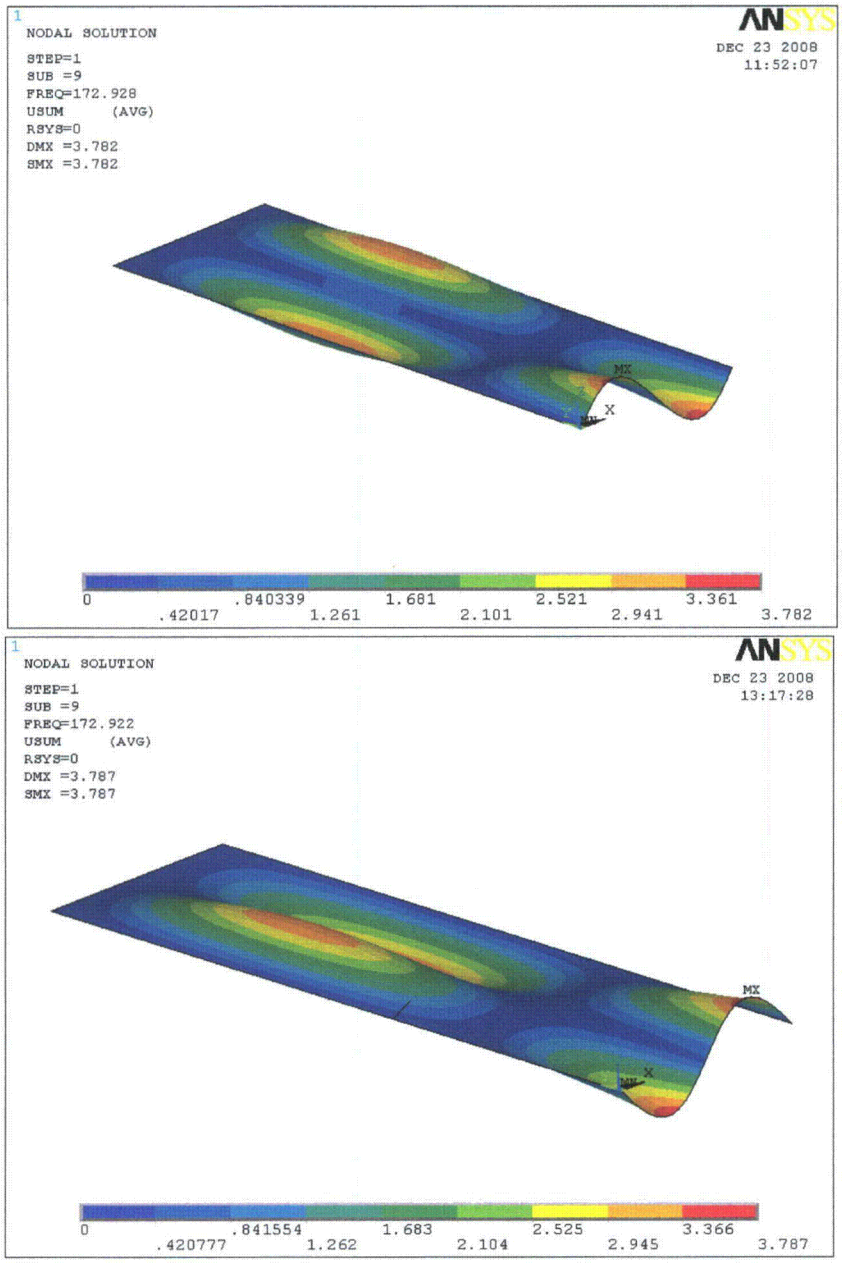

Figure 5-30. Modal Comparison Between Uncracked (Top) and Cracked (Bottom) Panels, Mode 9, x/H=0.4, a/W=0.1.

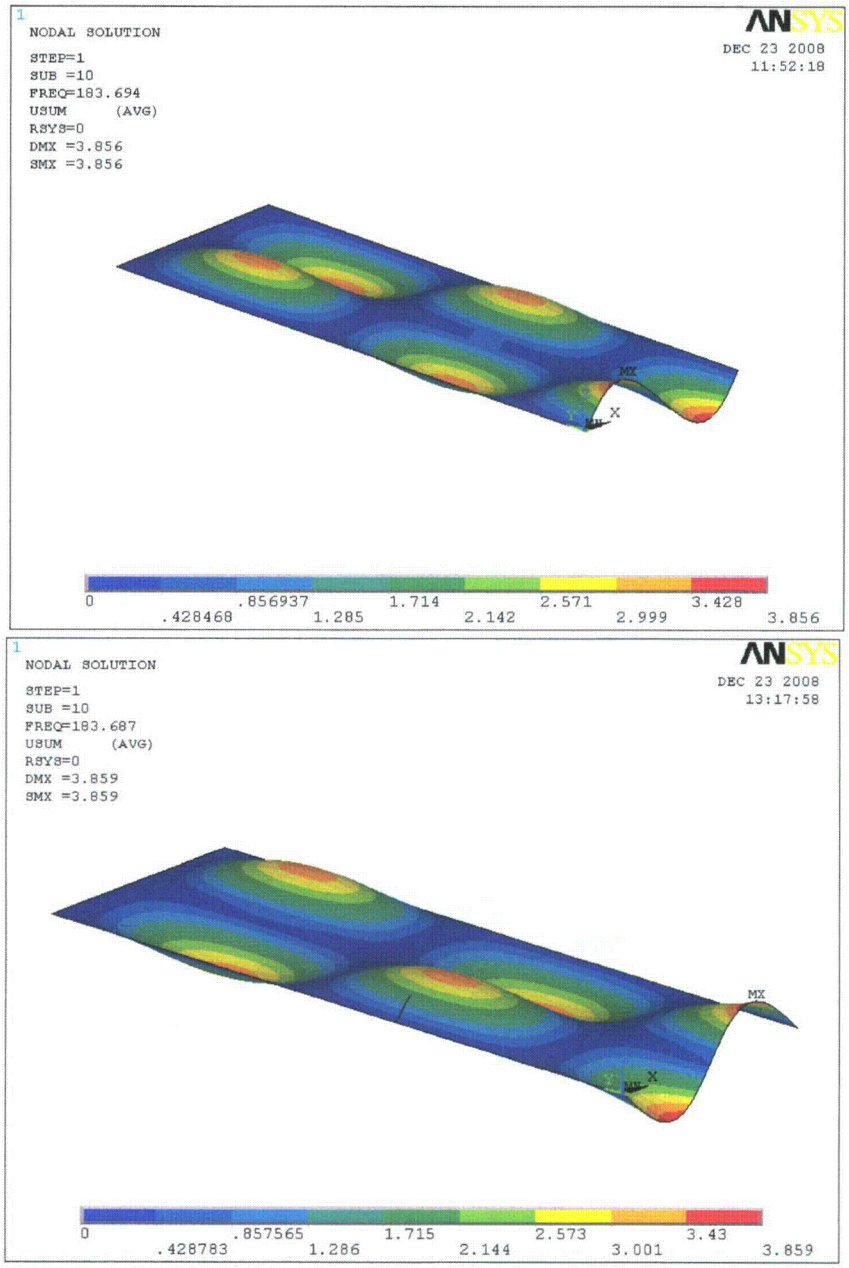

Figure 5-31. Modal Comparison Between Uncracked (Top) and Cracked (Bottom) Panels, Mode 10, x/H=0.4, a/W=0.1.

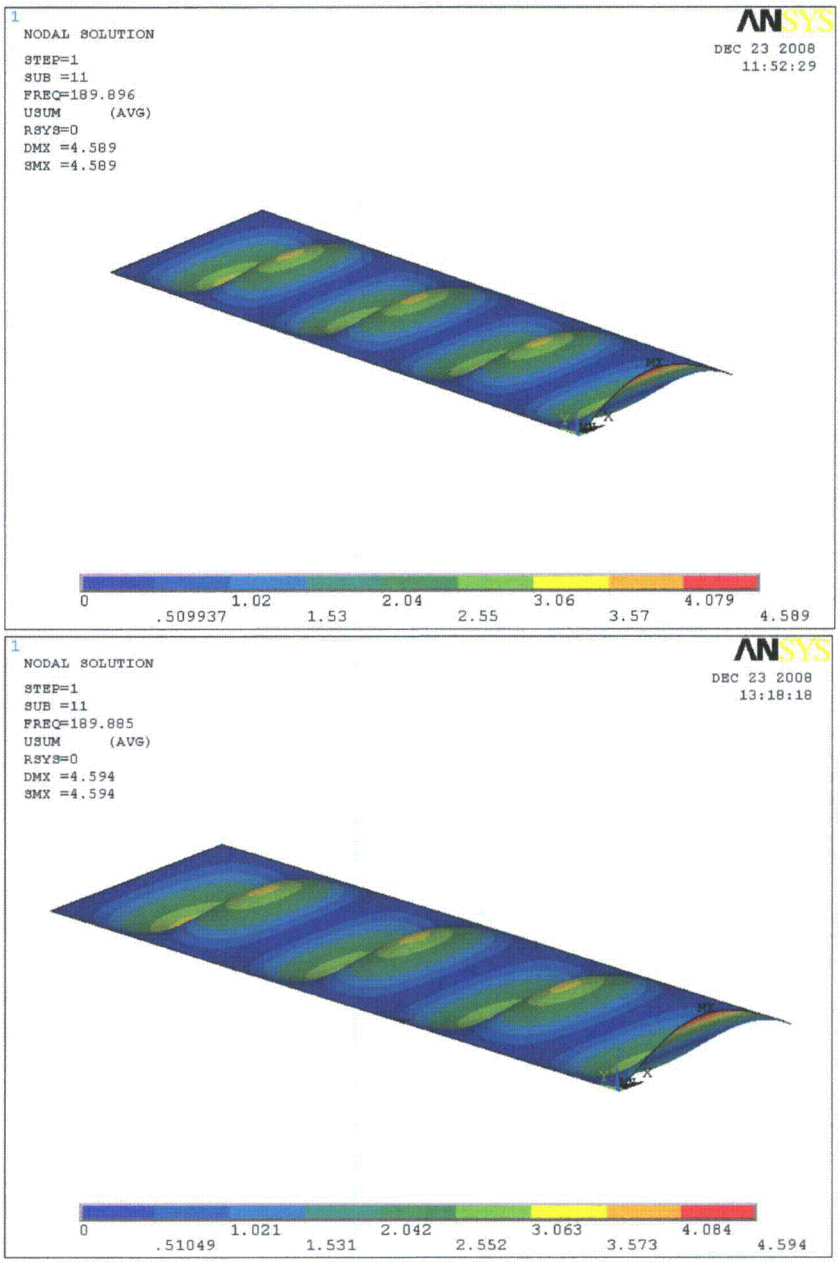

Figure 5-32. Modal Comparison Between Uncracked (Top) and Cracked (Bottom) Panels, Mode 11, x/H=0.4, a/W=0.1.

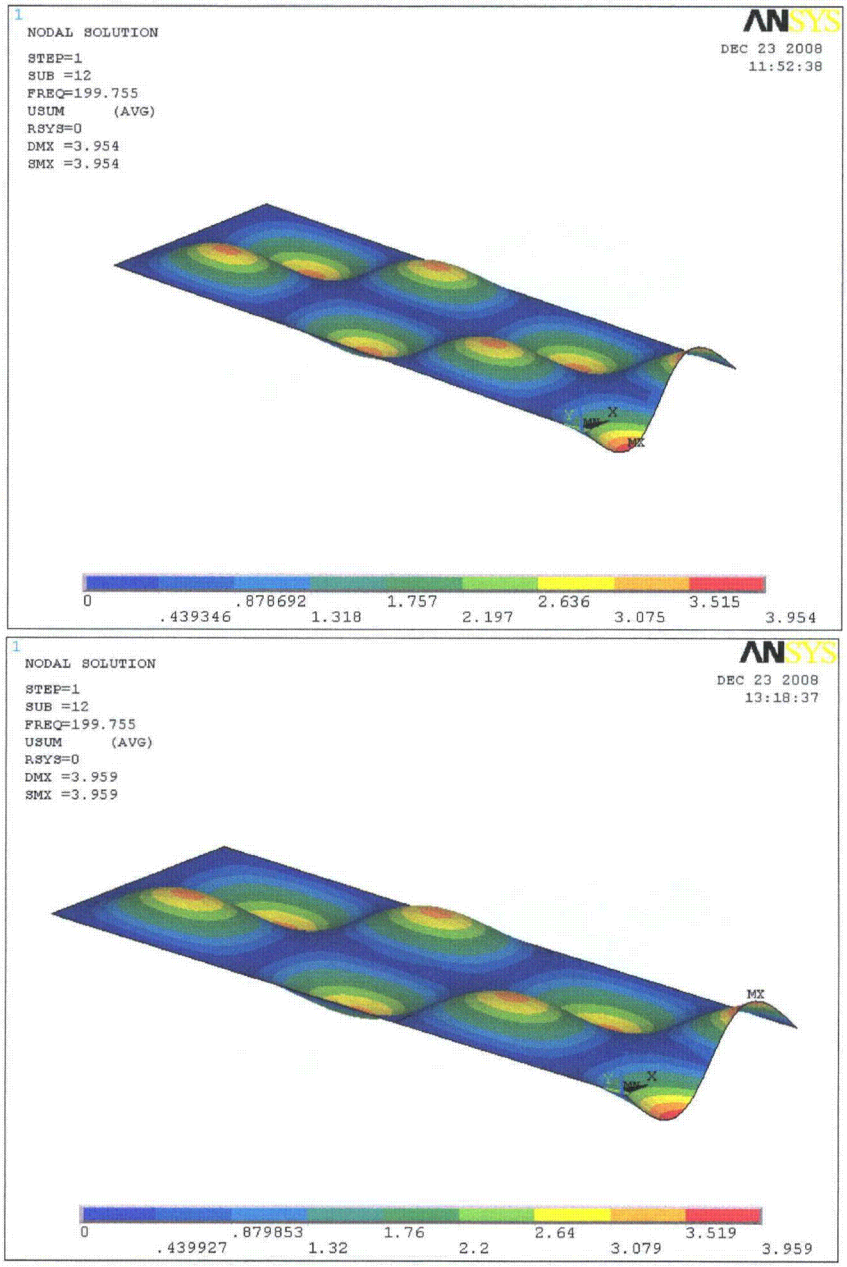

Figure 5-33. Modal Comparison Between Uncracked (Top) and Cracked (Bottom) Panels, Mode 12, x/H=0.4, a/W=0.1.

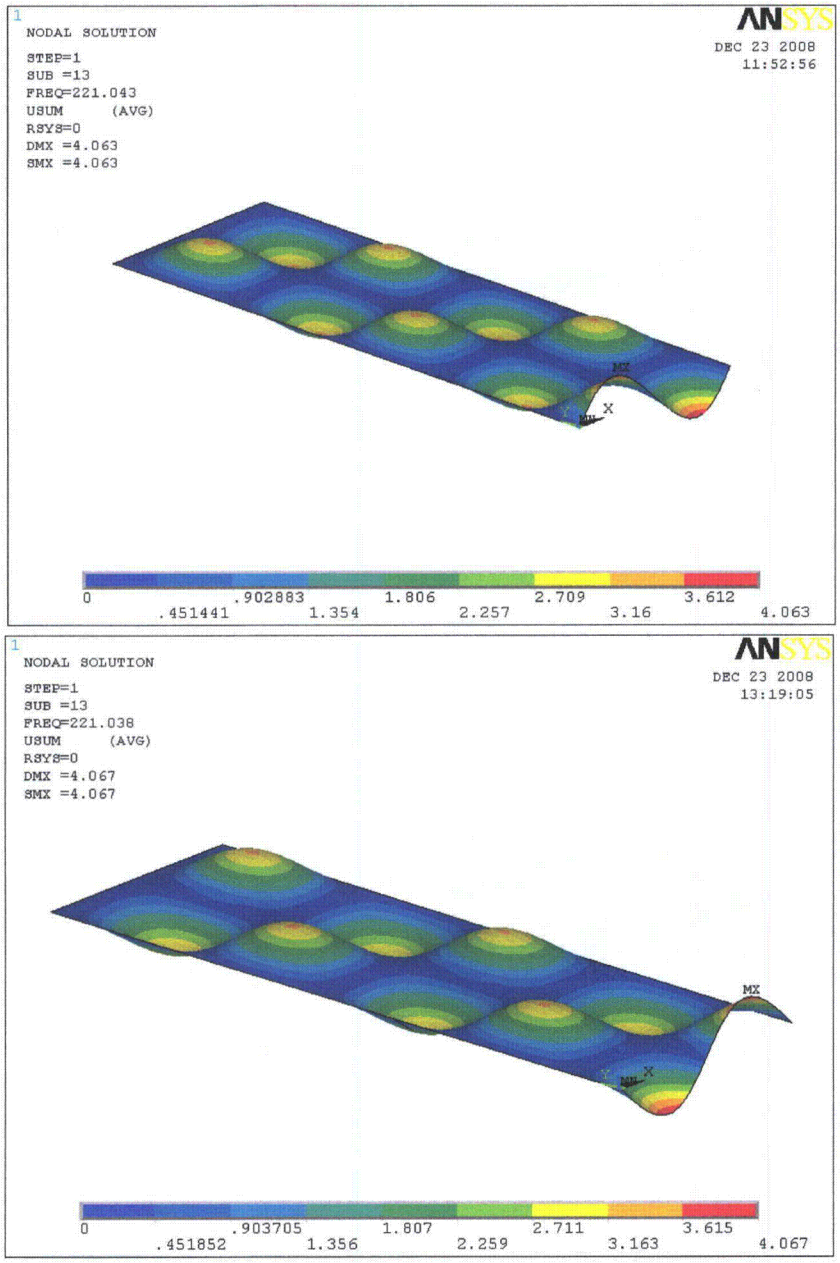

Figure 5-34. Modal Comparison Between Uncracked (Top) and Cracked (Bottom) Panels, Mode 13, x/H=0.4, a/W=0.1.

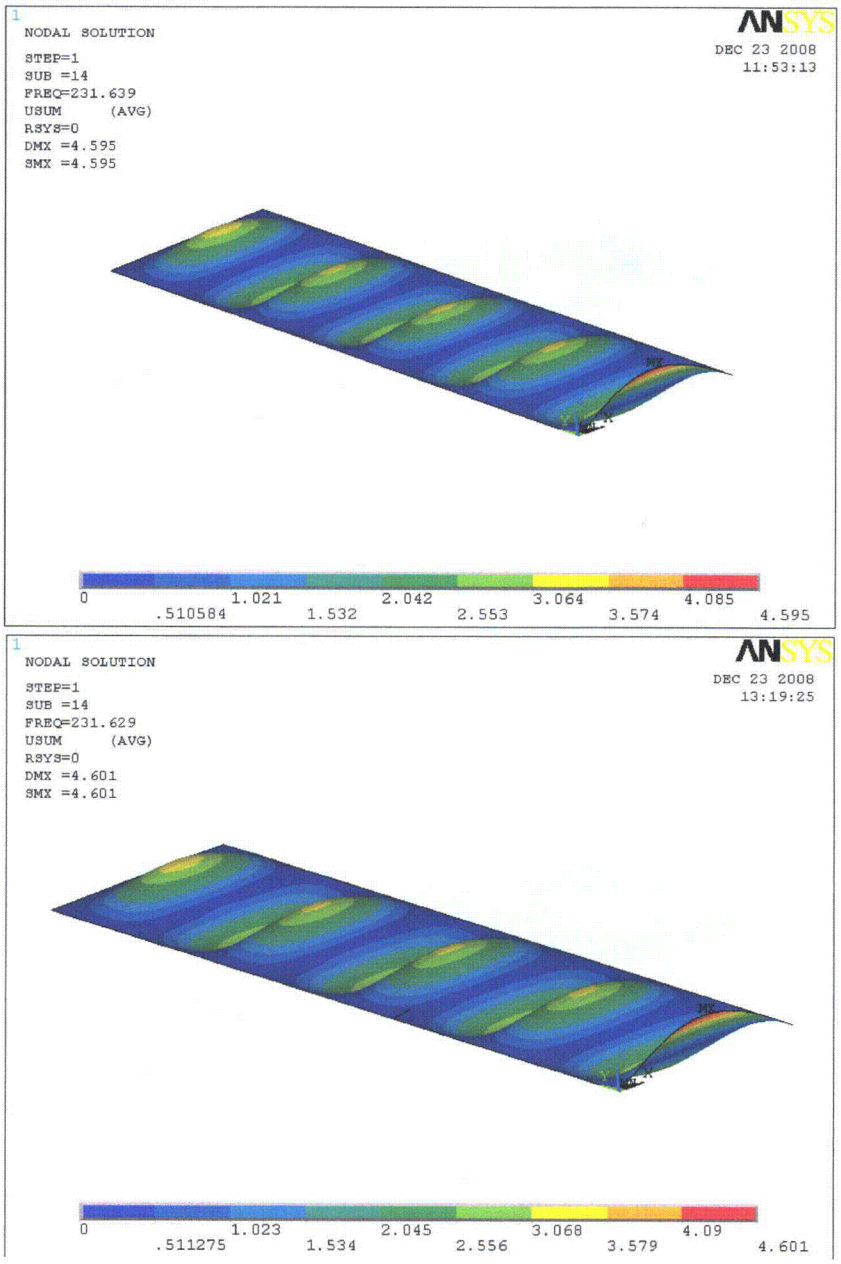

Figure 5-35. Modal Comparison Between Uncracked (Top) and Cracked (Bottom) Panels, Mode 14, x/H=0.4, a/W=0.1.

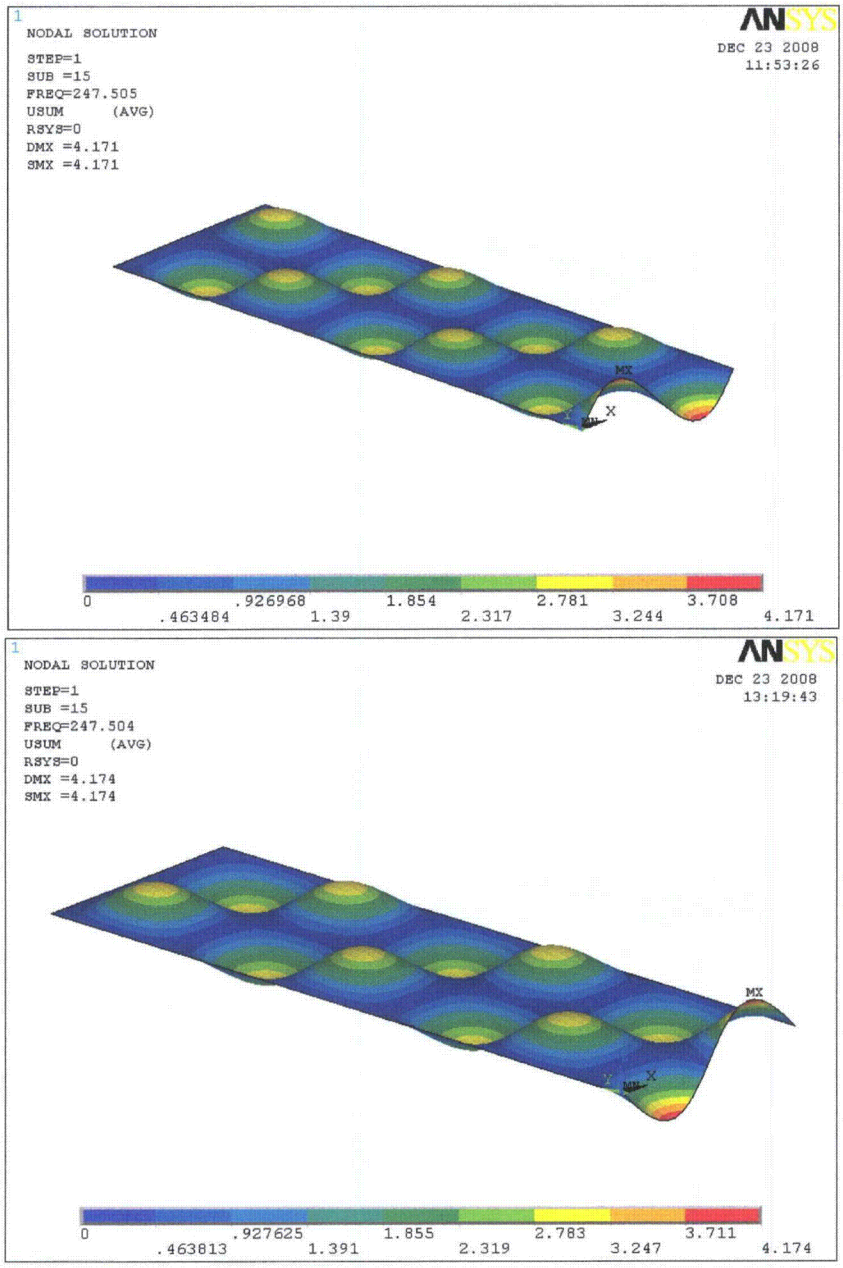

Figure 5-36. Modal Comparison Between Uncracked (Top) and Cracked (Bottom) Panels, Mode 15, x/H=0.4, a/W=0.1.

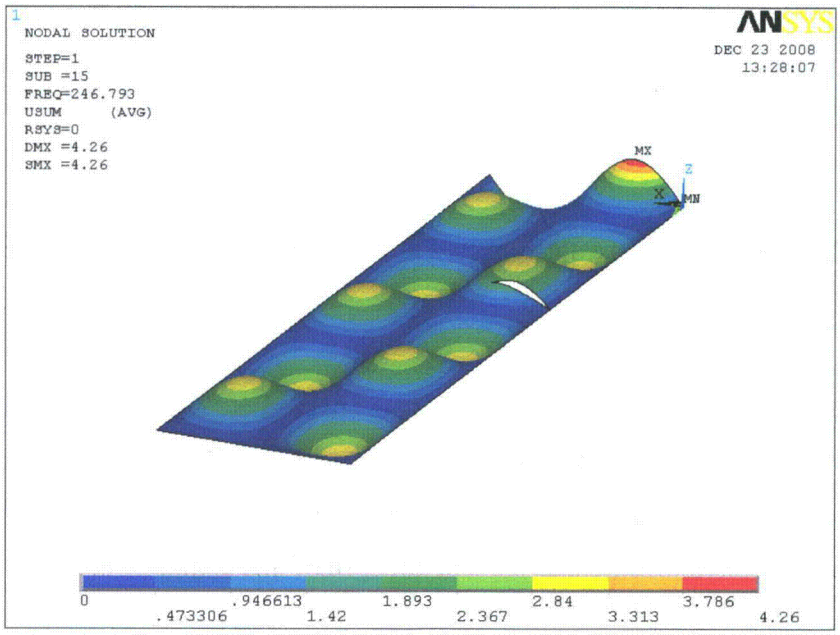

Figure 5-37. Modal Comparison Between Uncracked (Top) and Cracked (Bottom) Panels, Mode 15, x/H=0.4, a/W=0.3.

6.0 CONCLUSIONS

Considering the results of this evaluation and the operating experience for this and other BWR steam dryers with similar indications, the following conclusions are made:

1. The subject indications are not expected to exhibit significant further fatigue crack growth.

2. The IGSCC indications in upper support ring are predicted to experience further IGSCC growth; however, the end of cycle flaw sizes remain small compared to the section thickness and the ligament remaining at the end of the next operational cycle is adequate to react the applied loading and prevent collapse of this component.

3. None of the indications considered in this evaluation have the potential to create loose parts during the next operational cycle.

4. All indications should be inspected during the next refueling outage to identify any additional crack growth.

5. The cracking observed in the NMP2 steam dryer will not affect the vibration response of the steam dryer sufficiently such that the FEM created for the EPU stress analysis needs to be modified to incorporate cracking.

7.0 REFERENCES

1. "Invessel Visual Inspection (IVVI) of Reactor Pressure Vessel Components for the Nine Mile Point Unit 2 Nuclear Station During the Spring 2008 Outage," Report No. G9MI2-N2R11-309718, April 2008, Westinghouse, SI File No. 0801273.201.
2. Design Inputs from Constellation Energy Group. SI File No. 0801273.204.
3. IVVI Inspection Photographs from Constellation Energy Group. SI File No. 0801273.202.
4. BWRVIP139: BWR Vessel and Internals Project, Steam Dryer Inspection and Flaw Evaluation Guidelines, EPRI, Palo Alto, CA, 2005. 1011463.
5. "Nuclear Engineering Report Nine Mile Point Unit 2: Miscellaneous Reactor Pressure Vessel Internals Inspections and Evaluations," NER-2M-078, Revision 6, August 2007. SI File No. 0801273.204.
6. Design Inputs from Continuum Dynamics, Inc. **CDI Proprietary Information**. SI File No. 0801273.203P.
7. ASME Boiler and Pressure Vessel Code, Section XI, 2004 Edition.
8. J.C. Newman and I.S. Raju, "Stress Intensity Factor Equations for Cracks in Three-Dimensional Finite Bodies," ASTM STP 791, Volume I, ASTM, Philadelphia, 1983, pp. I281-I296.
9. Tada, Hiroshi, and Paul C. Paris, George R. Irwin. The Stress Analysis of Cracks, 3rd Edition. New York: ASME, 2000.
10. GE-NE-0000-0027-5624-01, Revision 1. April 2004. **GE-H Proprietary Information**. SI File No. 0801273.204P.
11. Young, Warren C. and Richard G. Budynas. Roark's Formulas for Stress and Strain, 7th ed. New York: McGraw-Hill, 2002.
12. Meirovitch, Leonard. Fundamentals of Vibrations. New York: McGraw-Hill, 2001.
13. Blevins, Robert D. Formulas for Natural Frequency and Mode Shape. Florida: Krieger Publishing, 2001.
14. ANSYS, Release 8.1 (w/Service Pack 1), ANSYS, Inc., June 2004.
15. GE-H Services Information Letter 644, "BWR/3 Steam Dryer Failure," August 21, 2002.